uc3m | Universidad Carlos III de Madrid

SCHOOL OF ENGINEERING

Bioengineering and Aerospace Engineering Department

Biomedical Engineering

DEVELOPMENT AND VALIDATION OF A 3D-PRINTED PHANTOM FOR IMAGE GUIDED LAPAROSCOPIC SURGERY

Author: Alexis Pomares Pastor
Tutor: Mónica García Sevilla

In collaboration with:

Hospital Universitario Gregorio Marañón
SaludMadrid
Comunidad de Madrid

BIG BIOMEDICAL IMAGING AND INSTRUMENTATION GROUP

Título: **Development and validation of a 3D-printed phantom for image-guided laparoscopic surgery**

Autor: **Alexis Pomares Pastor**

Tutor: **Mónica García Sevilla**

EL TRIBUNAL

Presidente:

Vocal:

Secretario:

Realizado el acto de defensa y lectura del Trabajo de Fin de Grado el día _ de _ de 2018 en Leganés, en la Escuela Politécnica Superior de la Universidad Carlos III de Madrid, acuerda otorgarle la CALIFICACIÓN de:

VOCAL

SECRETARIO PRESIDENTE

Abstract

Surgical training and research depend on either clinical, animal or phantom studies. The first two options provide the most realistic environment, but they present serious ethical, economic and regulatory barriers. Phantoms provide a consistent, cost-effective solution, especially advantageous for use in early stages of device development or medical training. When combined with specific training software, they constitute an effective learning platform for disciplines such as image-guided surgery or minimally invasive procedures.

Several training systems based on the use of phantoms have been developed for a variety of applications, from open-source platforms for training of ultrasound-guided needle insertions, to virtual reality applications that simulate the environment of an operating theatre. OpenHELP is an open-source project in which a modular 3D-printed phantom was created for laparoscopic surgical training and evaluation, based on the segmentation of a full-body computed tomography scan of a patient.

The goal of this project was to develop a thorough system for training of laparoscopic skills, including: (i) an anthropomorphic torso phantom based on the OpenHELP dataset, with special focus on inexpensiveness and customization possibilities, and (ii) a realistic image-guided surgery setup for real time navigation and recording of activity.

Fused deposition modelling 3D printing technology was used to produce the full-scale torso –comprised of thorax, pelvic and chest parts– and reusable organ molds, employed for silicone casting and generation of the organs. Artificial skin was also created for the abdominal area, consisting of a 3D-printed framework and an ethylene-vinyl acetate foam sheet. An optical tracking system (OptiTrack Duo) and retroreflective fiducial markers were used together with the visualization software Slicer for navigation of the phantom.

Two subjects evaluated the perceived level of realism and accuracy of the system. The results proved that all components of the full-scale phantom fit together seamlessly, and the training software effectively allowed real-time navigation of the phantom. Despite minor flaws in calibration that caused occasional overlapping of models in the Slicer scene, the system was reported to provide a realistic feeling of immersion. A future work guideline could be conducting these tests with a wider group, including specialized participants such as medical students or experienced surgeons.

Acknowledgements

Quiero dar las gracias a todas las personas que me han ayudado a lo largo de la carrera.

A mi familia, por su apoyo incondicional y por estar siempre ahí.

A Mónica, por haber sido una magnífica tutora, por su gran dedicación, y por ayudarme en las tediosas luchas contra la silicona.

A Javier Pascau, por haber sabido valorar mi trabajo y brindarme una oportunidad, tanto para realizar las prácticas, como con este Trabajo de Fin de Grado.

A toda la gente del departamento de bioingeniería de la UC3M y del HGUGM que me ha ayudado, directa o indirectamente, con el desarrollo de este proyecto.

A los chavales, por distraerme de vez en cuando.

Gracias a todas y todos.

Acronyms

IGS – Image Guided Surgery

3D – Three-dimensional

OpenHELP – Open Heidelberg Laparoscopic Phantom

MRI – Magnetic Resonance Imaging

ELITE – Endoscopic-Laparoscopic Interdisciplinary Training Entity

EMT – Electro-Magnetic Tracking

CT – Computed Tomography

SLS – Selective Laser Sintering

CAD – Computer-Aided Design

FDM – Fused Deposition Modelling

SLA – Stereolithography

PLA – Polylactic Acid

PVA – Polyvinyl Alcohol

STL – Standard Triangle Language

EVA – Ethylene-Vinyl Acetate

AR – Augmented Reality

Contents

List of figures

List of tables

1. Introduction

1.1. Laparoscopic surgery

Laparoscopy is a kind of surgery conducted in the abdominopelvic region (depicted in *Figure 1.1*), characterized by the use of small incisions (~ 0.5-1.5 cm) and the assistance of a camera –laparoscope– as an alternative to the traditional open procedure [1]. As a result, it achieves reduced pain and hemorrhaging, and faster recovery times.

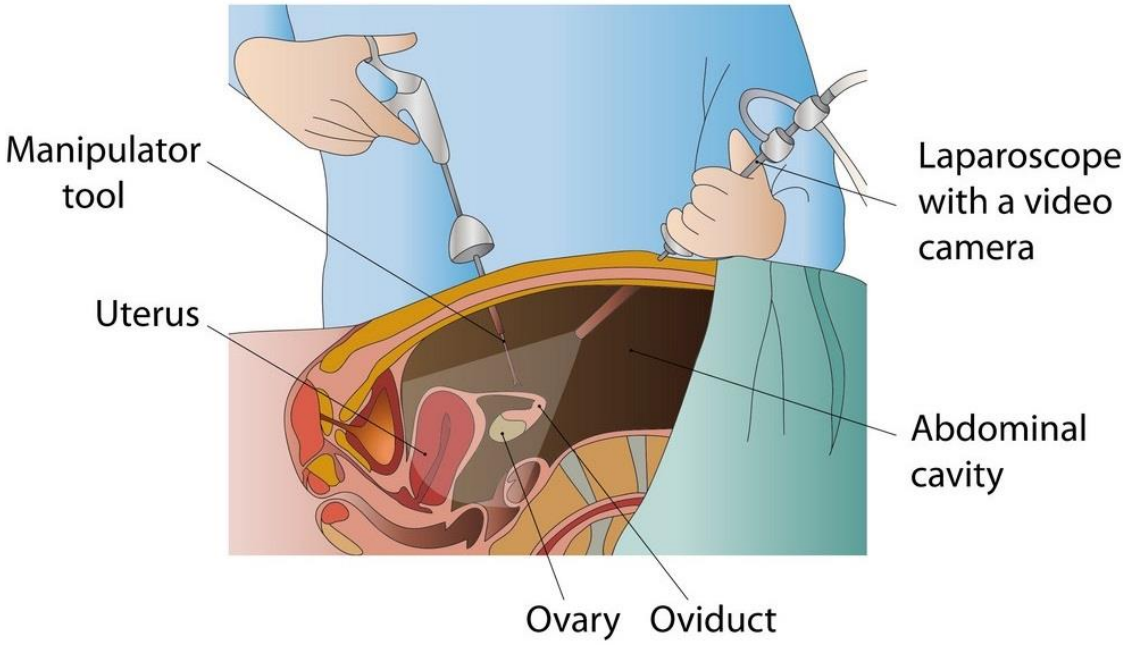

Figure 1.1. Schematic of gynaecological laparoscopy [2].

Despite the evident benefits of laparoscopic surgery in the matter of patient outcomes, the drawbacks mainly come from the increased difficulty of the procedure [3]: the surgeon has a restricted range of motion, poor depth and tactile perception, they need non-intuitive tool manipulation skills, and there is a specific associated risk related to blind insertion of the trocar, which may lead to abdominal injuries [4].

Consequently, the surgeon needs to acquire a high degree of dexterity and a particular set of skills [5], as happens with many other surgical procedures. Since it would be risky to let students have their first experiences with real patients, in its place, animals, cadavers or medical phantoms are typically employed.

1.2. Medical phantoms

Medical phantoms –or simply, phantoms– are specially designed devices used for surgical training of students, as well as for evaluation of new medical imaging technologies prior to testing with real patients (*Figure 1.2*).

Figure 1.2. Anthropomorphic torso phantoms for surgical team training (left) and for CT –computed tomography– scan tuning and analysis (top) [6, 7].

Their main advantages: they are more readily available, consistent, and ethically innocuous than the abovementioned living subjects, animals or cadavers. On the other side, they are usually expensive, unsuitable for certain applications and short-lived [8, 9].

1.3. Surgical training software

Training software provides objective feedback and helps ease the learning curve of surgical trainees. Its use has become more popular in recent years, with several virtual/mixed/augmented reality applications being actively developed and employed in the operating theater [10, 11, 12], as illustrated in *Figure 1.3* and *Figure 1.4*.

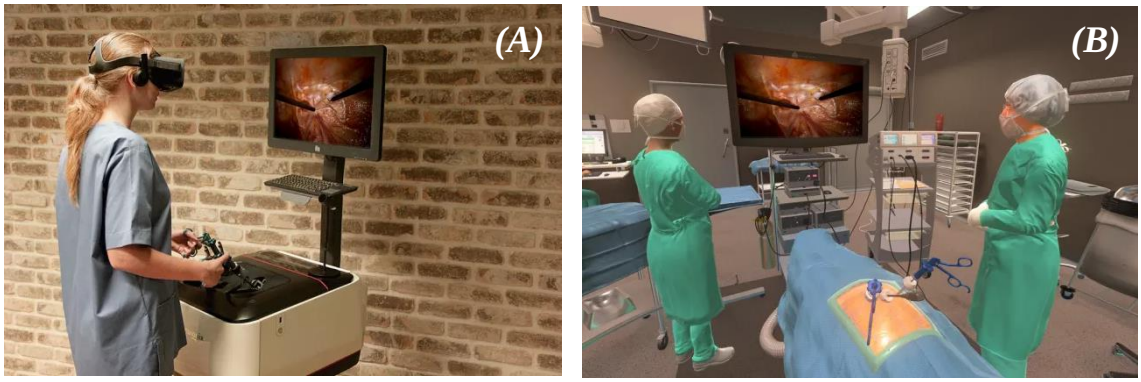

Figure 1.3. Virtual reality simulation of: (A) Camera vision of laparoscopic surgery, with realistic force feedback; (B) Operating room environment [13].

Figure 1.4. Virtual reality surgical training, with a mentor observing the performance of the trainee, and the tools being tracked with fiducial markers. [14].

This software enables a realistic recreation of specific scenarios, and the recording of student's activity for later revision, which translates into more flexible, customized and efficient training procedures [15, 16].

1.4. Image-guided surgery

Image-guided surgery (IGS) tracks surgical instruments in real-time and uses this information together with pre- or intra-operative images to support the procedure (*Figure 1.5*). This technology allows the surgeon to better control their movements with respect to the patient's anatomy, resulting in improved safety, invasiveness, and speed [17].

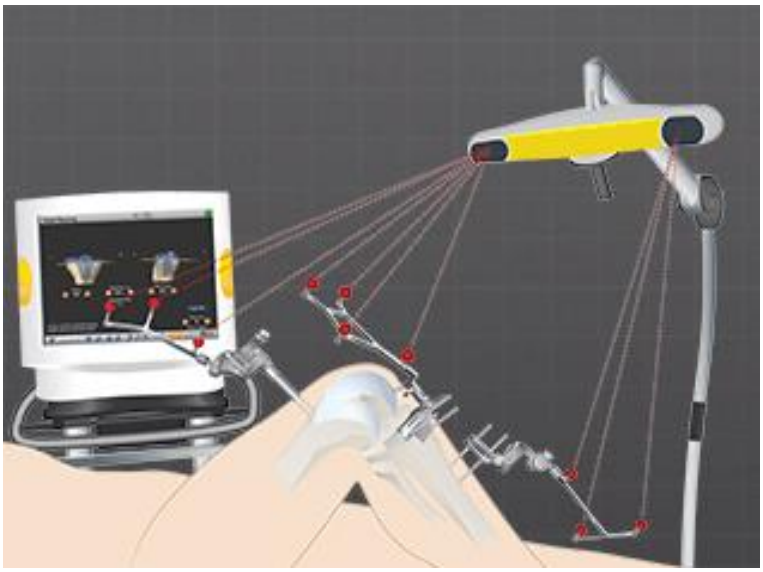

Figure 1.5. Schematic of real-time tracking in image-guided knee surgery [18].

IGS is also of prominent value for surgical training. It allows accurate assessment of the student's performance when handling surgical tools with respect to the phantom structures (see *Figure 1.6*), using positioning systems for real-time feedback [19].

Figure 1.6. Illustration of tool tracking inside patient in image-guided spine surgery [20].

1.5. 3D printing in the medical environment

The term '3D printing' encompasses multiple techniques for creating three-dimensional objects by additively joining or solidifying material in consecutive layers (*Figure 1.7*). It enables the fabrication of customized objects with complex shapes or geometries, which would be unachievable using any other methods. Typically, 3D digital models of the object are sliced in layers of small thickness (~ 0.1mm) using specific software, and materialized by successively depositing one layer on top of another.

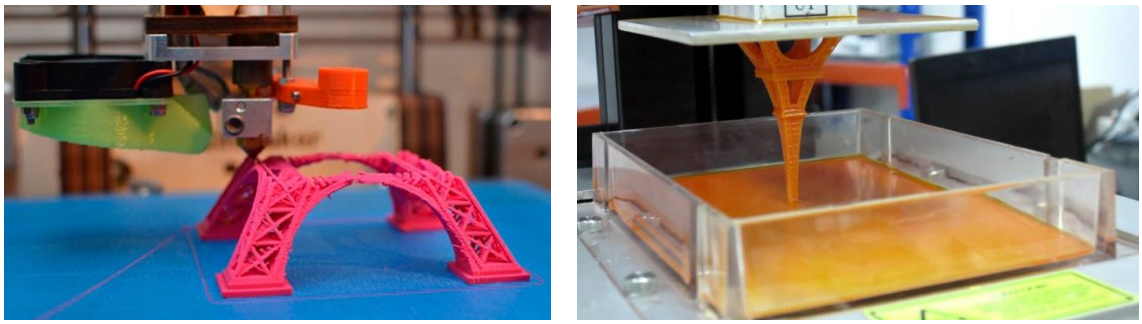

Figure 1.7. Fused deposition modelling (left) and stereolithography (right) 3D printing techniques [21, 22].

The medical industry has largely benefited from the inexpensive customization potential offered by 3D printing techniques. Numerous applications for diverse medical disciplines

have emerged in the recent years, such as microfluidics (*Figure 1.8*), personalized implants and anatomical models (*Figure 1.9*), or cell bioprinting (*Figure 1.10*).

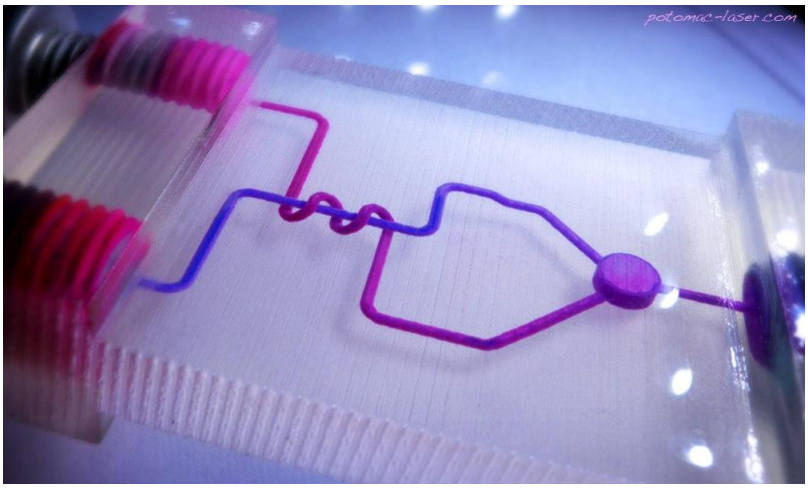

Figure 1.8. Low-cost, rapid 3D-printing of microfluidic device [23]

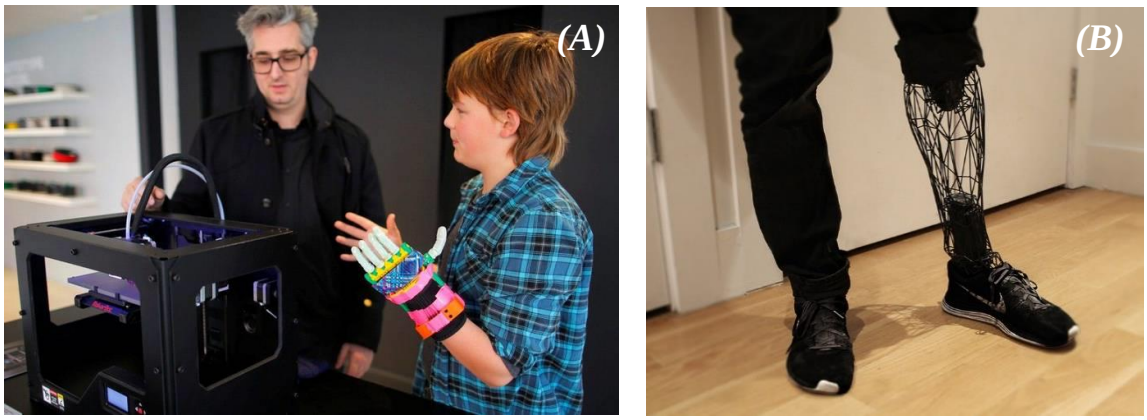

Figure 1.9. (A) Mechanically functional 3D-printed hand prosthesis, characterized by its low production cost [24]. (B) Titanium dust 3D-printed leg prosthesis, which achieves lightweight, resistant results [25].

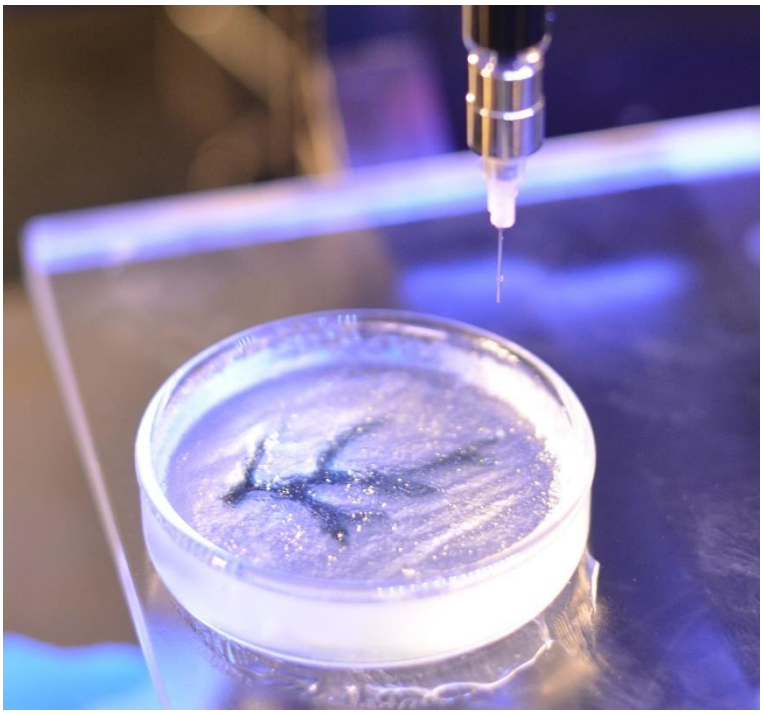

Figure 1.10. Bioprinted coronary artery, embedded in a gel-like scaffold [26].

2. Motivation

Clinical training and evaluation of new medical devices currently rely on three main solutions (see *Figure 2.1*): clinical trials, animal experiments and phantom studies, the former being clearly considered gold standard. However, clinical trials entail high costs, complex experiments, and may pose ethical concerns, which makes them not feasible for early stages of training and medical device development [27, 28, 29].

Figure 2.1. Clinical research approaches: (A) clinical, (B) animal and (C) phantom studies [30, 31, 32].

Animal experimentation provides realistic anatomy and surgical workflow similar to humans, but it is still cost intensive, it requires an animal testing license, and it may be ethically not justifiable [33, 34].

On the other hand, phantoms can be easily manipulated, and do not pose any ethical barriers [35]. State-of-the-art phantoms accurately reproduce the human anatomy, tissue properties and patient motion (e.g. breathing), as illustrated in *Figure 2.2*. When combined with the use of specific software, they constitute a powerful tool for surgical training of medical students.

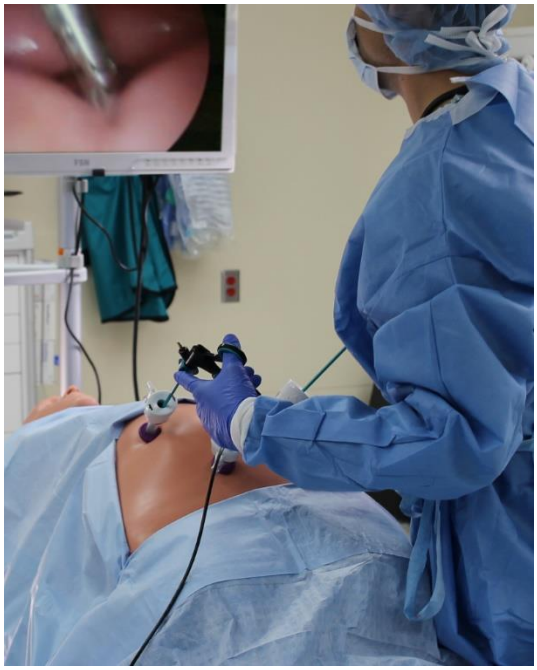

Figure 2.2. Surgical trainee performing a laparoscopy on anthropomorphic phantom [6].

However, cutting-edge phantoms are substantially expensive solutions, more even if they are adapted for certain operating procedures, such as minimally invasive or image-guided surgery. The most economical phantoms often lack realism, or are designed for single use and are not suitable for regular applications. Furthermore, the use of specific software is frequently subject to copyright and license fees, which impose an additional economic burden and restrict the possibility to develop code for customized applications [36].

In view of this, the aim of this project was the thorough development of a system for laparoscopic training, consisting of: (1) a cost-effective, easily reproducible, modular and reusable phantom with accurate haptic and anatomical properties, and (2) a realistic image-guided surgery setup based on the use of free, open-source software. For the production of the phantom itself, we based our work on the open-source project Open Heidelberg Laparoscopic Phantom (OpenHELP) [35].

3. State of the Art

In this section we will be reviewing the state-of-the-art of every field relevant to our project. These include: medical phantoms, image-guided laparoscopy, surgical training software and medical 3D printing. As it is the main point at issue, special emphasis will be placed in the application of phantoms to these fields.

3.1. Phantoms

The use of medical phantoms began soon after the discovery of X-rays by the German physicist Wilhelm Röntgen in 1895. X-rays quickly became popular for its multiple, novel applications, in what would be the very first steps of an entire new medical discipline, the science of radiology. However, when the hazards associated to ionizing radiation were realized, a need for substitutes of living tissue was evident. In this way, the concept of phantoms was born [36].

The earliest phantoms were quite modest in their design, consisting of water tanks or wax blocks that would enable simple measurements of radioactive sources. It would not be until the 1960s that realistic, more sophisticated anthropomorphic phantoms would begin to be developed, such as the Resusci-Anne phantom for simulating human ventilation and training of cardiopulmonary resuscitation [37].

Around this time, and with the accelerated development of computers, a new approach for simulating the human body was conceived: computational phantoms [38], which are mathematical models that allow computerized simulations of the human body. They have been, and still are, widely employed in the field of radiology, from ionizing radiation dosimetry studies to nuclear medicine.

Over time, the design of medical phantoms has been refined to accurately reproduce numerous features of the human body. While medical phantoms were originally used to study 2D imaging techniques (e.g. radiography, or fluoroscopy), today they serve for a wide variety of applications, such as: performance analysis and tuning of new medical

devices; research, testing and validation of 3D imaging techniques; and support for new operating procedures and for medical training of students [9, 28, 35].

The purpose for which phantoms have been devised will completely determine their design and composition. They can be either bought as commercial products, or self-developed for research, as is the case of this project.

For example, the research breast phantom developed by Keenan et. al. [39] was designed for quantitative evaluation of magnetic resonance imaging (MRI) protocols. It achieves critical physical properties for this imaging modality by using corn syrup solution and grapeseed oil, which effectively mimic the relaxation behavior of glandular and fatty tissues, respectively. This keeps the production costs and complexity low, while maintaining its functionality, which is why it has been frequently used for optimization and standardization of breast MRI imaging protocols, as in [40]. Nevertheless, the phantom is lacking numerous features that would make it valuable for multiple other clinical settings, which were sacrificed to preserve its crucial inexpensiveness.

On the other hand, the medical device manufacturer Kyoto Kagaku commercializes a cardiopulmonary motion phantom [41], consisting of a human-like torso with skeletal structure, heart and diaphragm. The motion of the latter two can be programmed with several parameters, such as respiration/heart rate, volume, etc. This phantom has a wide array of applications, e.g. correction of misregistration artifacts in chest radiographies [42]; yet, it is somewhat inaccurate in the representation of the real motion of the organs.

3.1.1. Phantoms for laparoscopic surgery

The endoscopic-laparoscopic interdisciplinary training entity (ELITE) trainer by Gillen et. al. [43] is a commercial anthropomorphic torso with latex visceral organs, designed for both laparoscopic and endoscopic training. It has been widely used in the context of these fields [44, 45], since it provides a complete, consistent and standardized solution. The main drawbacks are its elevated cost –a common trait of commercial phantoms [46,

47]– and the lack of possible customization, as opposed to other commercial solutions like the simulators of the medical technology manufacturer VirtaMed [48].

The OpenHELP (Heidelberg laparoscopy phantom) [35] is an open-source research phantom, composed of an anthropomorphic torso, pneumoperitoneum, and silicone organs. It was designed to be easily reproducible and modular, with its torso divided in three: upper, lower and chest. Both the torso and the set of organs were materialized via 3D printing, and as it is an open-source project, all of its data is accessible in the public domain [49]. This makes it particularly useful for research applications [50, 51], because it allows to completely adapt the phantom to the exact needs of the study. Disadvantages are the rather elaborate production process of most components, and the need for further development, including the removal of magnets for attachment and the lack of motion simulation.

3.2. Image-guided surgery

The origins of IGS trace back to the 1900s, when stereotactic neurosurgical techniques were developed. Nevertheless, it would not be until the 1990s that they started to be routinely used, and it has been since progressively adopted in many surgical standard procedures, evolving together with computers, 3D imaging modalities, and tracking systems [52].

Today, IGS is based on the use of preoperative imaging (usually a computed tomography –CT– scan) to track surgical tools and display them in a screen with regards to medically important structures, such as bones or nerve tissue [53].

As a curiosity, positioning systems such as the ones used in IGS have found application in many different fields and disciplines, a notable one being the cinematographic industry. They are frequently employed for capturing the movements of actors in animation films, or even for videogames.

3.2.1. Positioning systems

The most frequently used tracking systems are the optical ones, which employ fiducial markers (e.g. infrared retroreflective spheres, or actively emitting diodes) to track the position in space of surgical tools [54]. This method has seen little variation over the years, as it is a simple, effective and inexpensive technique. Still, it has disadvantages, remarkably the possibility of occlusions and physical interference with the activity of surgeons, and the effect of markers geometrical configuration on the overall accuracy of the system [55].

Several alternatives have emerged which may be more suitable for determined situations. For instance, electromagnetic tracking systems do not require direct line of sight and can track flexible instruments [56], contrary to the traditional optical systems. The main drawback presented by electromagnetic tracking is the susceptibility to interference generated by tools made of ferromagnetic materials, which restrict their possible applications [57].

Another interesting method was proposed by Chae et. al. [58], based on afocal optics. It uses lenses and micro-engraved data-coded patterns, which implies smaller size markers and improved efficiency and accuracy of the tracking system. However, it has only been tested *in vitro*, so it remains to be validated with *in vivo* experimentation.

3.2.2. Training software

Software-based platforms are an important resource for medical education, yet its use is not so widespread amongst the surgery community. A study by Maertens et. al. [11] performed an exhaustive literature search, and analyzed the results of 87 randomized controlled trials with almost 8,000 participants total. These studies had in common that they compared the efficacy of e-learning platforms (for example, multimedia interactive learning, virtual patients, virtual reality environments and simulations…) against either a different method of training, or no training at all. They concluded that, despite significant

variation for different types of platforms, e-learning was overall equally or more effective than other methods for surgical training.

Several other studies have arrived at similar conclusions [10, 59, 60], showing that computer-based tools have a strong potential and, in the future, they will be standard in the field of surgical training.

3.2.3. Phantoms for image-guided laparoscopic surgery

IGS has also promising future in laparoscopic surgery; given the limited amount of visual and haptic/tactile information available to the surgeon –due to the minimally invasive nature of the approach–, IGS could greatly assist in the procedure. For instance, thanks to intraoperative visualization of body structures, the risk of iatrogenic nerve damage can be notably reduced [61].

Wagner et. al. [62] studied the feasibility of electromagnetic tracking (EMT) of organs for real-time compensation of tissue shift in image-guided laparoscopic surgery. This is a promising alternative to the regular intraoperative imaging, which is frequently not viable for many operating procedures. For the study, they evaluated three different scenarios with varying degrees of compensation, using the OpenHELP phantom and an EMT organ sensor. Combining both preoperative imaging (a CT scan of the phantom) and intraoperative EMT, they achieved encouraging results, with the most complex model having a tracking error of 2.9 ± 1.4 mm. Thus, they proved that electromagnetic organ tracking can be effectively used to compensate for the infamous iatrogenic tissue shift.

3.3. 3D printing in the medical environment

Given the changing and singular nature inherent to different medical cases, the cost-effective customization possibilities offered by 3D printing technologies are revolutionizing health care [63, 64, 65]. They have found numerous applications in diverse medical settings, including –but not limited to–: custom-made implants,

prosthetics and anatomical models; tissue and organ bioprinting; microfluidics; surgical planning and sterilizable tools fabrication…

Phantoms are also largely benefited from the advances in 3D printing, providing a competitive substitute for commercial phantoms when these are too expensive or not adequate for the needs. Selective laser sintering (SLS) is a common choice for printing of rigid body parts, such as the torso or bony structures [35, 66]. On the other hand, reusable organ molds are usually printed in gypsum to pour silicone in and obtain the organ models. Polymeric materials are also popular to produce flexible phantoms, which are often employed to study specific conditions and diseases related to soft tissue, e.g. abdominal aortic aneurysm [67].

In conclusion, medical 3D printing is rapidly evolving and disrupting the market, with quick scientific and regulatory adaptations emerging as the technology, and its usage, progresses. Several initiatives are already start-up to accelerate research and implementation, like the '3D Print Exchange' website of the National Institutes of Health for downloading and sharing of 3D print files and educational materials [68].

4. Materials and methods

4.1. Data acquisition

As it has been previously mentioned, the production of the phantom was based on the open-source project OpenHELP [35]. The dataset is available on their website [49], which contains segmented 3D models from an anonymized male patient CT scan of the torso and of the organs. The former can be downloaded as a whole or as individual chest, upper, and lower parts, while the latter comprises the organs from the mediastinum (heart, lungs and trachea), abdomen (stomach, duodenum, pancreas, spleen, liver, rectum lumen and kidneys), and pelvis (bladder and pelvic muscles).

However, some errors were detected in the dataset, including distorted models and missing information on the procedures to be followed. After unsuccessful attempts of communication with the organization, a workaround had to be found for each of these obstacles, as will be discussed below.

4.2. Production of the torso

The 3D models were digitally manipulated using the free computer-aided design (CAD) program Autodesk Meshmixer. The pelvis (lower) and thorax (upper) parts were used as is from the OpenHELP dataset; the breast shield, however, was found to be erroneous, being of the order of 20 times smaller in size than what it should have been to properly match the thorax model. Upon scaling, it still was geometrically disfigured, making it impossible to fit in any configuration. Therefore, it had to be obtained by boolean subtraction of the pelvis ("*Torso_Lower_Part.stl*") and thorax ("*Torso_Upper_Part.stl*") from the whole-body model ("*Torso_Complete.stl*"), which included the chest area. Both the original and the generated chest plates are shown in *Figure 4.1*.

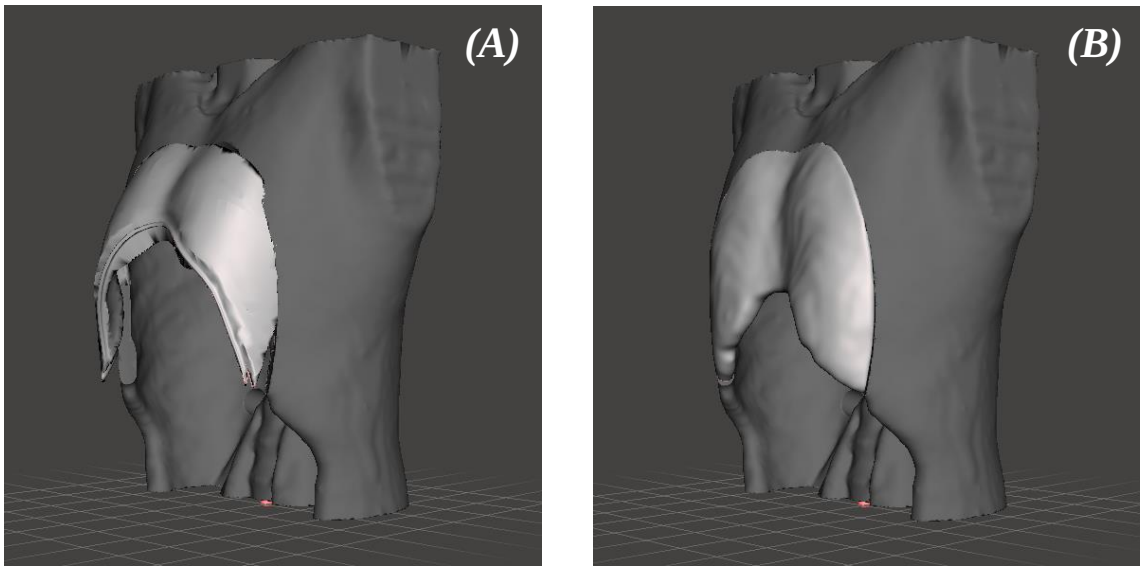

Figure 4.1. Fitting of the erroneous (A) and modelled (B) chest shields in the upper torso.

Once the models were ready, several additive manufacturing techniques were considered for materialization of the torso. A summary is presented in *Table 4.1* of advantages and shortcomings relevant to the requirements of the torso.

Table 4.1. Characteristics of 3D printing technologies [69, 35, 70].

Feature	*Fused deposition modelling (FDM)*	*Selective laser sintering (SLS)*	*Stereolithography (SLA)*
Durability	++	++	+
Print cost	€	€€ / €€€	€€
Accuracy	–	+	++
Print speed	–	++	+
Weight	+	+	+

Given the exceptionally large size of the models, it was deemed highly impractical to use the fused deposition modelling (FDM, described in *Figure 4.2*) printer at our university, as it would have taken excessive printing hours, and required subdivision of the torso into smaller pieces. In this way, the printing was conducted by an external company –Sicnova

3D, Madrid– via FDM (*Figure 4.3*). The chosen material was polylactic acid (PLA), a biodegradable, thermoplastic polymer with excellent mechanical properties commonly used in medical applications [71].

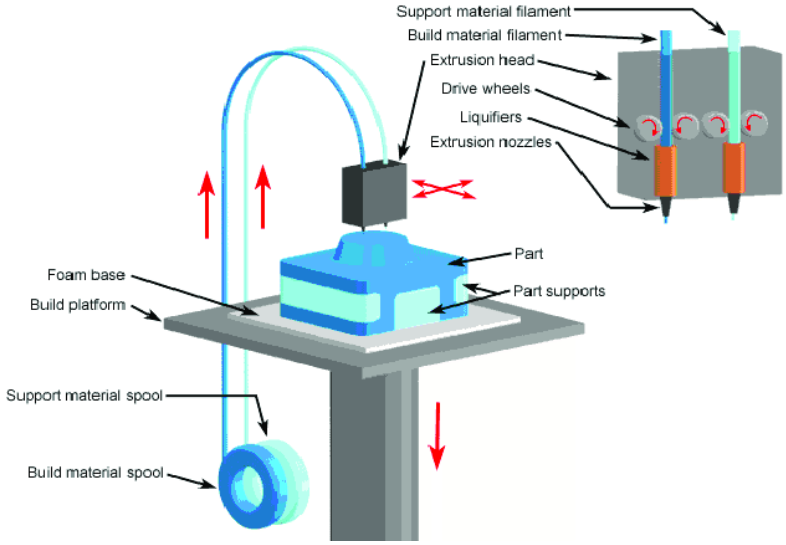

Figure 4.2. Schematic of FDM technology [72].

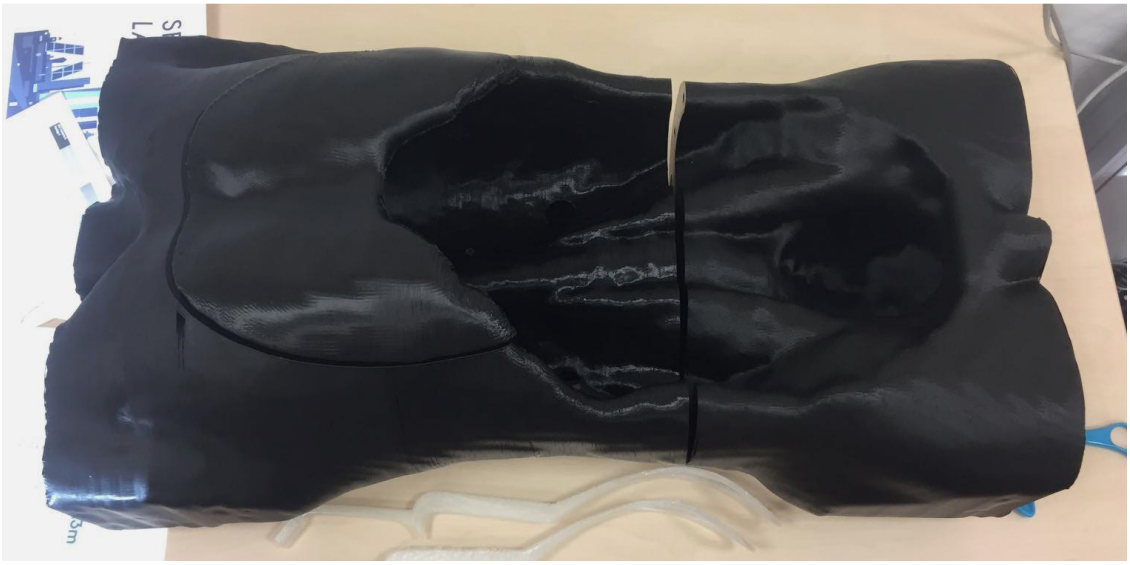

Figure 4.3. Full-scale 3D torso print in three parts: thorax, pelvis and reconstructed chest plate.

It has been stated that the modularity of the phantom was one of its main distinguishing features, offering the possibility to stay with only one half of the torso, or to remove the chest plate if desired. Since the scope of this project would always require the entire torso, and for pure convenience and manageability reasons, the pelvic and thorax parts were permanently affixed using cyanoacrylate glue.

4.3. Production of the organs

4.3.1. Modelling and printing of organ molds

For this section, a different approach from the OpenHELP project was taken. For the OpenHELP phantom, first the organs were printed in gypsum, then negative silicone molds were generated by using a polymethacrylate box and modelling clay, and later soft silicone was poured into the molds to form the organs.

This process is quite elaborate though, so instead it was decided to directly 3D-print the molds in PLA with a Ultimaker 3 Extended printer. This machine uses the FDM technique, which requires the addition of support structures for layer-by-layer formation of the object. The same PLA material can be used for the supports, but the preferred option –if a multi-extrusion 3D printer is available– is to choose another material, easier to remove after the print has been completed. Polyvinyl alcohol (PVA) was selected for this purpose, a water-soluble synthetic polymer frequently used in dual-extrusion 3D printing [73].

For the creation of the molds, the program Autodesk Meshmixer was employed to perform an offset of 5 mm thickness on the surface of the organs, obtaining a hollow object that would effectively act as a mold. These models were then cut with oblique planes so that they could be printed in separate parts, which was an indispensable point for later unmolding of the organs. The criteria for this step was to minimize the number of cuts, while producing individual models with simple geometry that would avoid trapped fragments of the organ inside the mold, or excessive adherence to the walls.

Afterwards, the molds were oriented as they would be later used, and holes were placed in the superior part so that silicone could be poured in. In an initial version, the holes had a cylindrical shape and a diameter of 10 mm; after printing and testing, they were refined to a conical shape with 10 mm inner and 15 mm outer diameters, which allowed a more fluid silicone flow, and a better adjustment to the tip of the funnels employed.

Additional considerations were regarded, such as introducing auxiliary holes of 5 mm diameter where the geometry of the models would require it (for example, areas where silicone would find it difficult to access by the effect of gravity), or adding support structures that would keep the molds stable while casting the silicone (see *Figure 4.4*).

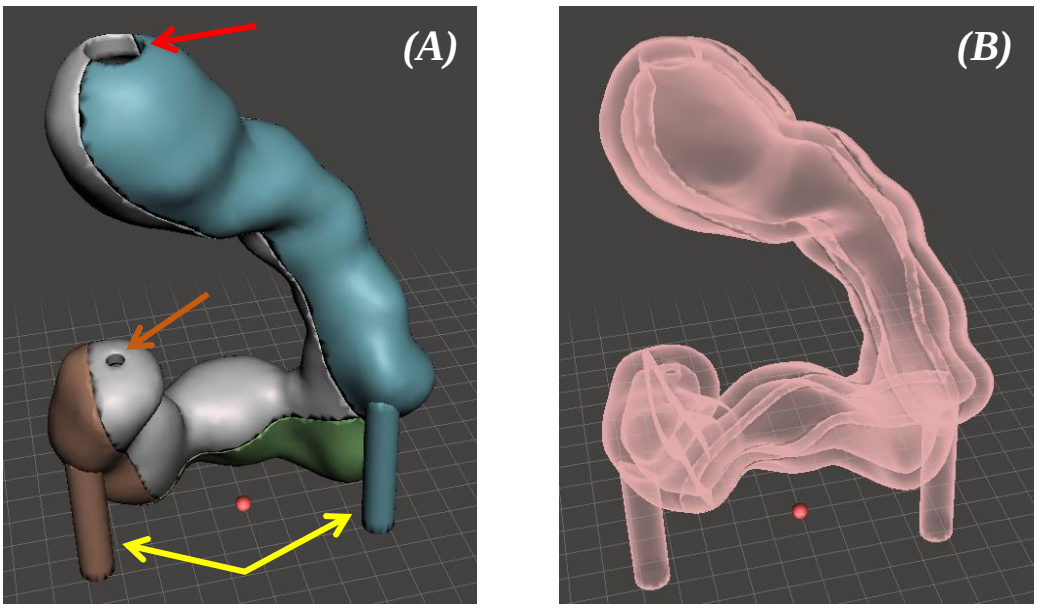

Figure 4.4. Duodenum mold. (A) Solid visualization with component parts in different colors, highlighting the silicone-pouring hole –red arrow–, auxiliary hole –orange arrow–, and support structures –yellow arrows–. (B) Translucent visualization, showing the duodenum-shaped interior of the mold.

Once the molds were finished, they were exported from Meshmixer as "Standard Triangle Language" (STL) files to import them into Ultimaker Cura, an open-source software application for 3D slicing and printing. They were sliced with a layer height of 0.2 mm, 10% infill, and oriented as in *Figure 4.5*, to ensure that the removal of supports would not affect the inner surface of the molds (which would later be the only interface with the silicone).

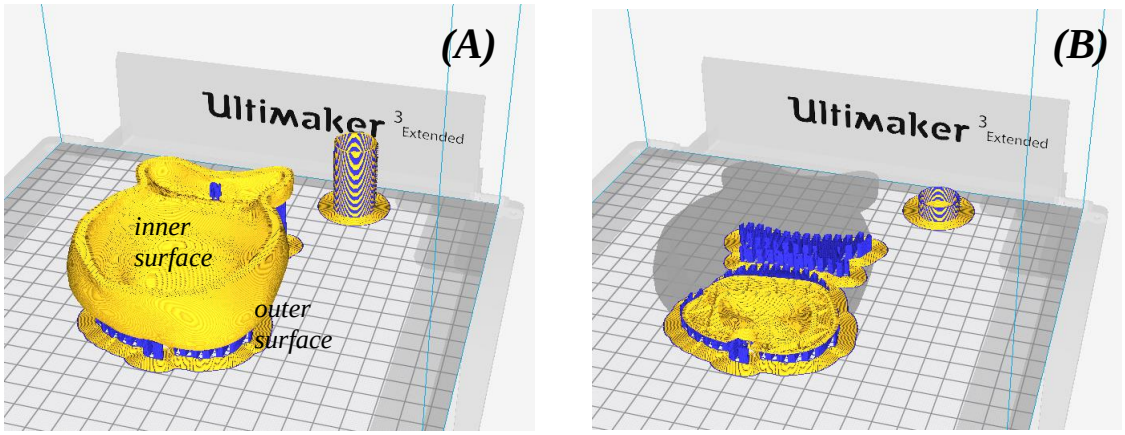

Figure 4.5. 3D-sliced upper half of the bladder mold, showing a preview of the last layer (A) and the beginning layers (B) of the print.

The STL files were then converted to g-code [74], and sent to the Ultimaker 3 Extended via Wi-Fi (*Figure 4.6*). After 3D printing, they were post-processed to remove the support structures by submerging them in warm water, at around 30 ºC for 6-12 hours. Due to time and printer availability constraints, only the organs from the abdominal and pelvic regions were materialized, which were deemed to have priority over the mediastinum organs (heart, lungs and trachea).

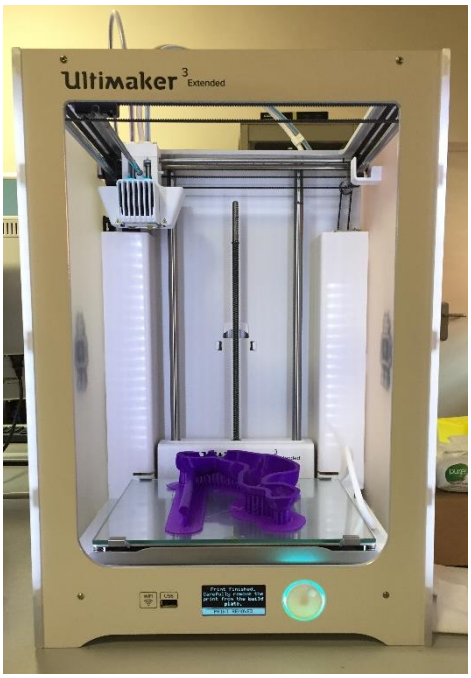

Figure 4.6. Finished 3D-print of the lower half of the stomach mold, where PVA support structures can be appreciated.

4.3.2. Mold casting and production of organs

In the OpenHELP report, it is mentioned that blends of three different silicones were employed to imitate the properties of real organs; however, they do not specify which proportion of each silicone was used for each organ. After unsuccessfully trying to contact the organization for further information, it was decided that precise reproduction of features such as stiffness or color was not strictly required for our project.

Only two types of silicone with different hardness and without mixing were used: Smooth-On Ecoflex 00-10 and Ecoflex 00-30 [75, 76]. Additionally, the silicone pigment FFX S-301 Light [77] was initially added to some organs, but its use was ceased for the reasons explained previously.

The silicones came as two separate constituents, named Part A and Part B. They were dispensed into a container with a 1:1 weight ratio, and stirred for 3 minutes to ensure that both parts were properly mixed. Adhesive tape was used to attach the different parts of each mold. Once already mixed, the silicone was poured into the molds with the help of a funnel, keeping a uniform flow to minimize entrapped air. It was allowed to cure at room temperature, and the organs were unmolded. This whole setting is illustrated in *Figure 4.7*.

It should be mentioned that the OpenHELP dataset does not include digital models of the bowels, because the intestinal walls were not recognizable in the CT scan and they were not segmented. For this reason, the intestines were not in the scope of this project.

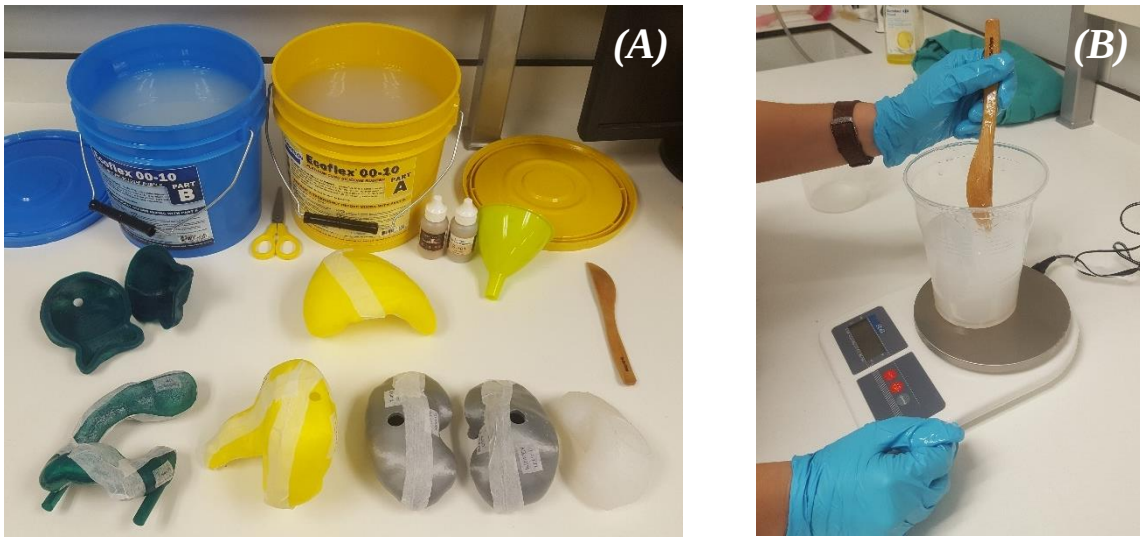

Figure 4.7. Production of the organs. (A) Setup for mold casting, including: parts A and B of the Ecoflex 00-10 silicone; FFX Light pigment; detached bladder and attached spleen, duodenum, stomach and kidney molds; and cured silicone kidney next to its mold. (B) Weighing and mixing of the silicone.

4.4. Production of the abdominal cover

A cover was specifically designed and modelled to perfectly fit the abdominal aperture of the phantom, whose purpose was to act as a structural base for the placement of a skin-mimicking ethylene-vinyl acetate (EVA) sheet. Instead of a solid infill, a grating pattern was conceived for the cover, such that holes to introduce the laparoscopic tools could be easily drilled.

The abdominal plate was divided in six pieces so that each could fit in the 3D printer, and materialized in the same way as the organ molds. As opposed to the silicone molds, in this case the individual pieces would not need to be posteriorly separated, so they were permanently fixed using cyanoacrylate glue and adhesive tape. The artificial skin (craft foam EVA sheet, thickness of 2 mm) was shaped, cut, and attached to the abdominal shield using the same method. The result is shown in *Figure 4.8*.

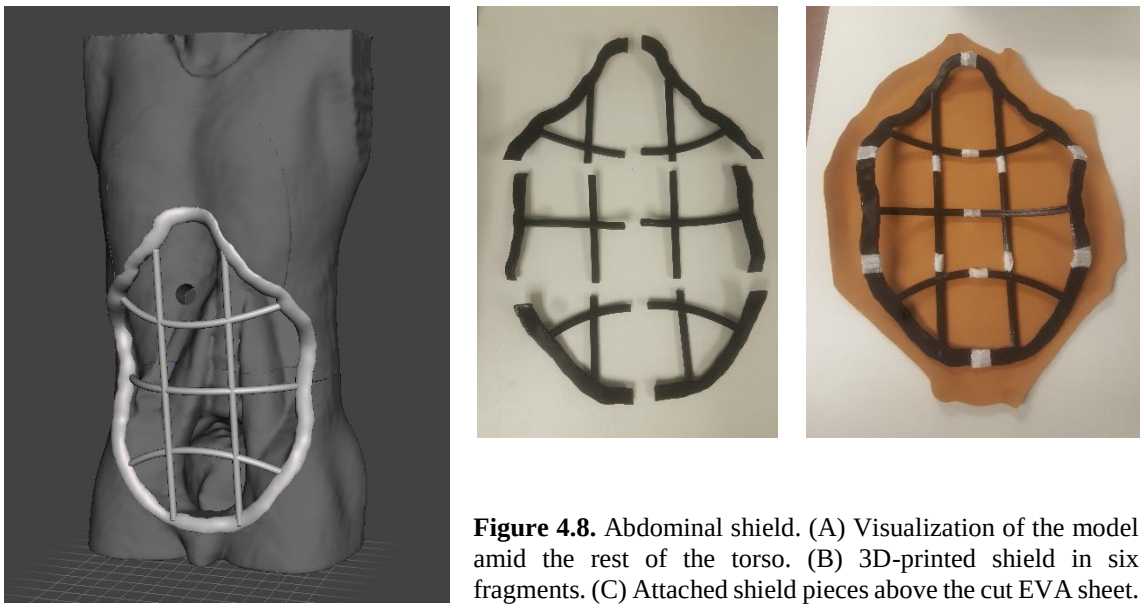

Figure 4.8. Abdominal shield. (A) Visualization of the model amid the rest of the torso. (B) 3D-printed shield in six fragments. (C) Attached shield pieces above the cut EVA sheet.

4.5. Preparation of the tracking system

4.5.1. Laparoscopic and tracking tools

A set of tools for laparoscopy were borrowed from our partner institution, the General University Hospital Gregorio Marañón, which comprised two Endo Clinch II 5mm trocars and one 3-Dmed T9 series Minimally Invasive Training System. The 3-Dmed simulator comes with various features and devices, from which the only relevant ones would be the 0° SimScope camera, and the monitor that displays the camera output.

As it has been discussed in section *3.2.1*, several options were contemplated for the positioning system. Since electromagnetic tracking is incompatible with the use of ferromagnetic tools, an optical tracking system OptiTrack V120:Duo was chosen, which was provided by the bioengineering department of University Carlos III of Madrid. Additionally, this optical system included a pointer tool with four fiducial markers integrated on it, useful for precise calibration and registration of the navigation system.

4.5.2. Rigid bodies and coupling pieces

The phantom and the navigation tools need to have fiducial markers (OptiTrack 6.4 mm M3 infrared retroreflective spheres) attached to them to be traceable by the OptiTrack device, as illustrated in *Figure 4.9*. These markers must have different angle configurations so that they are distinguishable from each other to the tracking system. Rigid body models were designed to host three fiducial markers each using the software Autodesk Fusion 360, with their respective dimensions shown in *Figure 4.10* and *Figure 4.11*.

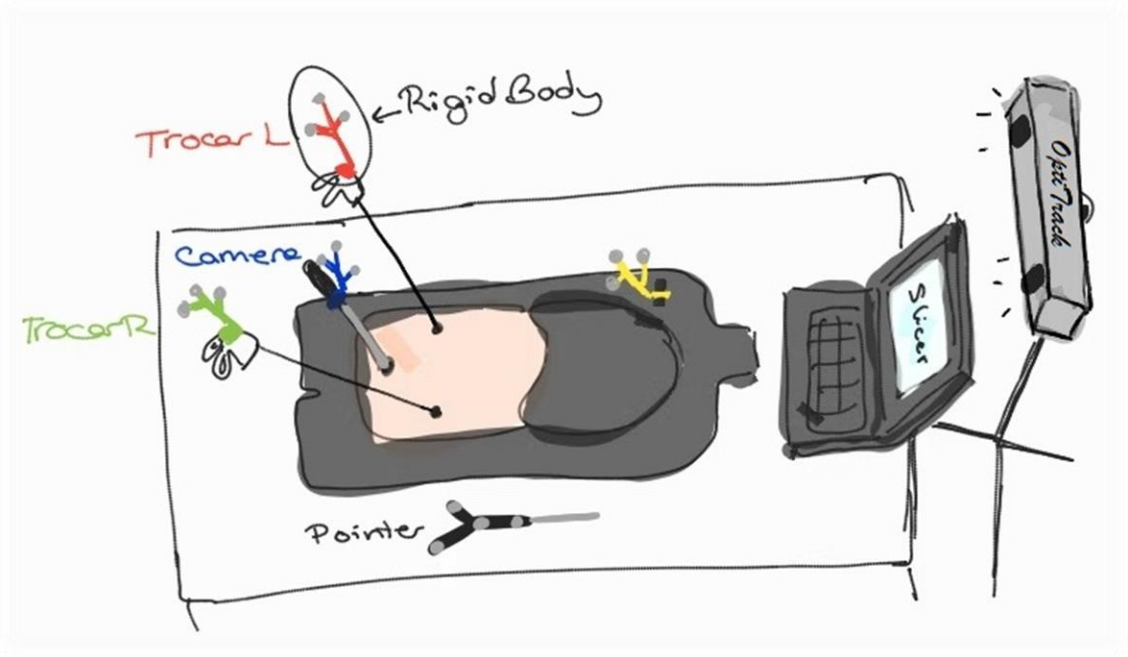

Figure 4.9. Sketch of the navigation system setup, showing detail of the phantom, the laparoscopic tools, the tracking system and the navigation software.

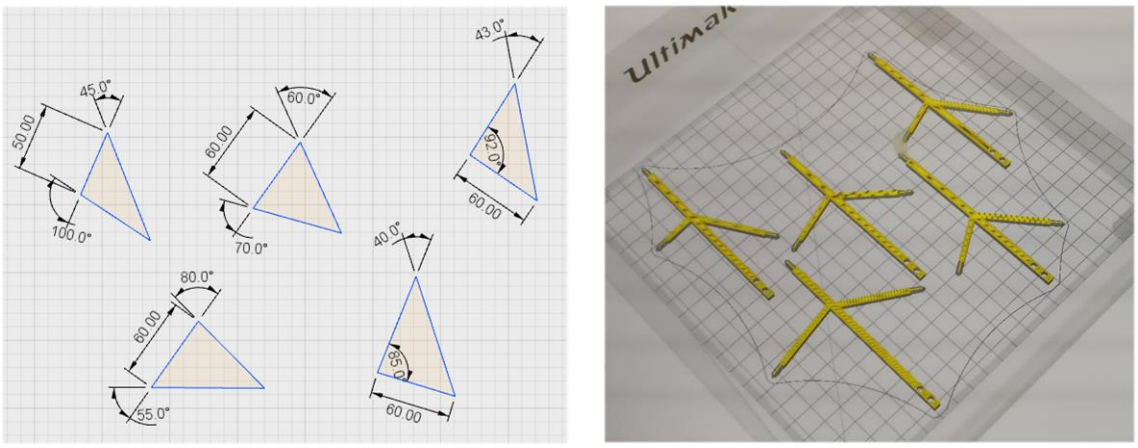

Figure 4.10. Schematic of the relative configuration of the fiducial markers for each rigid body (left), and distribution of the rigid bodies in the Ultimaker 3 Extended plate for materialization in one print (right).

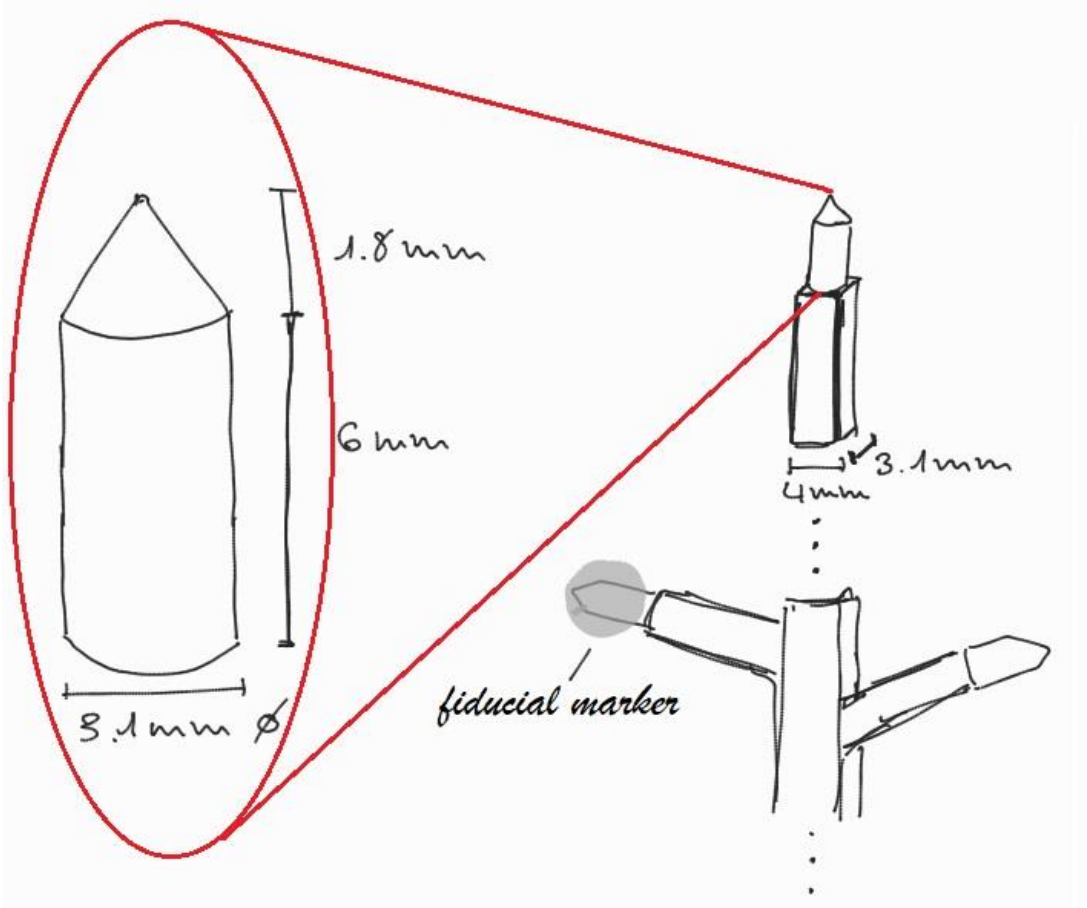

Figure 4.11. Sketch of the dimensions of the rigid body coupling tips, designed to precisely fit into the retroreflective spheres.

3D models of the navigation tools –i.e. the trocars and the camera– were also generated. Initially, a 3D surface scan was performed on them; however, the results were inaccurate and systematically presented several artifacts that turned them unusable. In view of this, it was opted to physically measure the tools and replicate them using the software Autodesk Inventor.

These models served two purposes: (i) visualization of the tools in the navigation software, and (ii) design of docking pieces tailored to the surface of tool handles, which would act as nexus between tools and rigid bodies (see *Figure 4.12*). These pieces were modelled using Inventor, with a small structure on the lateral with holes for screwing the rigid body and the coupling piece together.

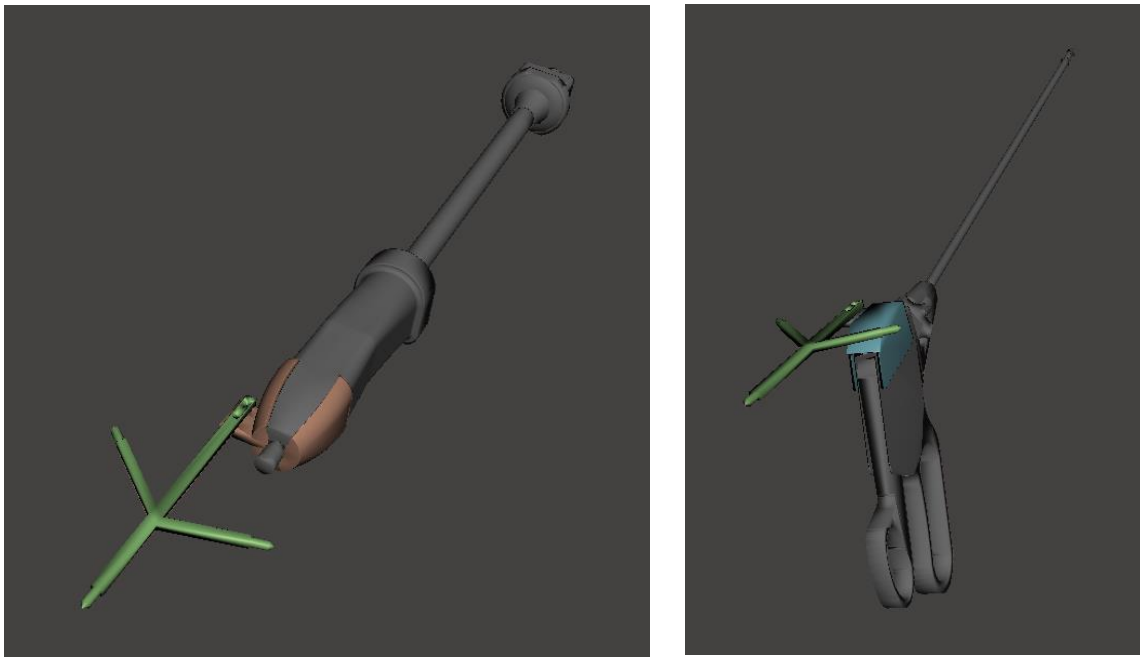

Figure 4.12. Visualization of the rigid bodies attached to the camera (left) and trocar (right) through the coupling pieces.

4.6. Training software

For the tracking and navigation, three software applications were used: OptiTrack Motive for motion capture and live-streaming of tracked rigid bodies; 3D Slicer for digital visualization and navigation; and Plus Toolkit for communication between Motive and Slicer. Two additional Slicer extensions were employed for navigation, namely Sequences –for recording of the activity in Slicer– and SlicerIGT –for phantom registration and laparoscopic tools calibration–.

An exhaustive list of all employed software programs is presented below, in *Table 4.2*.

Table 4.2. Summary of software applications used in the project

Purpose	***Software platform***
3D modelling and manipulation – Organic models	Autodesk Meshmixer
3D modelling and manipulation – Parametric models	Autodesk Inventor, Autodesk Fusion 360
3D slicing and preparation of models for printing	Ultimaker Cura
Motion capture and tracking of fiducial markers	OptiTrack Motive
Data communication between tracking and visualization software	Plus Toolkit
Visualization and recording of the motion of tracked objects	3D Slicer

4.7. Validation of the phantom and navigation system

Once it was ready, the whole laparoscopic training system was tested for validation. The phantom was horizontally positioned in a stretcher, the chest plate fixed with adhesive tape to the rest of the torso, and the artificial skin placed on top of the abdominal aperture. Four rigid bodies were affixed to the left and right trocars (*Figure 4.13*), to the camera and to the phantom. The pointer tool already came with fiducial markers incorporated on it, so the fifth rigid body was not needed. The OptiTrack camera was located so that its field of view would adequately fit the scene (*Figure 4.14*), leaving some margin for movement of the navigation tools around the phantom.

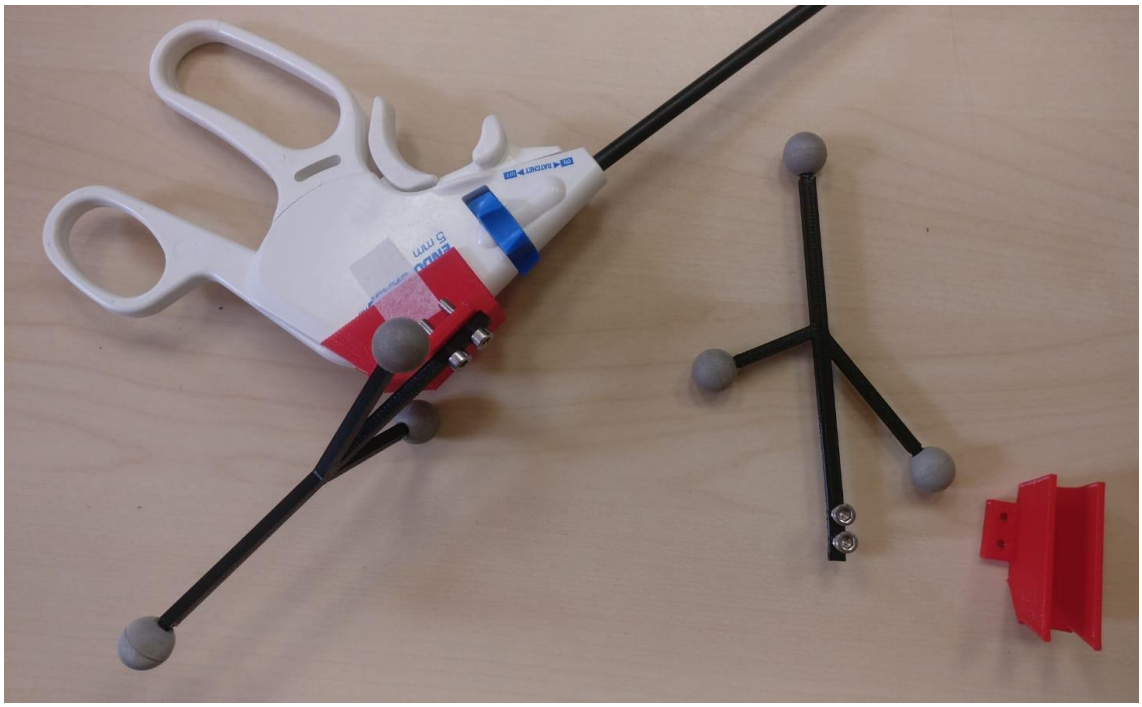

Figure 4.13. Detail of the union between rigid bodies and navigation tools.

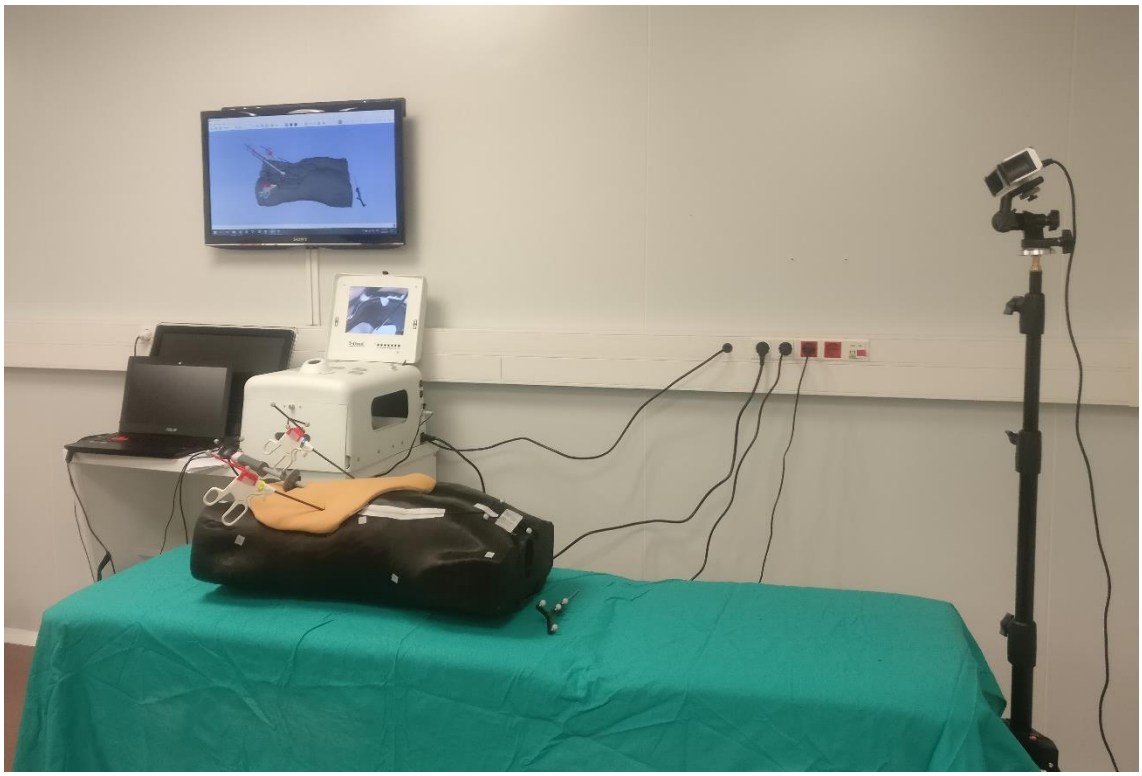

Figure 4.14. Navigation system setup, with laparoscopic tools introduced through the abdominal artificial skin. Observe that the scene is being faithfully reproduced in the screen on the background, without displaying the abdominal cover to allow visibility through it.

Figure 4.15 illustrates the overall workflow of the entire image-guided laparoscopic training system. The subjective perception of accuracy and realism were assessed by testing the system with two different subjects from the bioengineering department of the university.

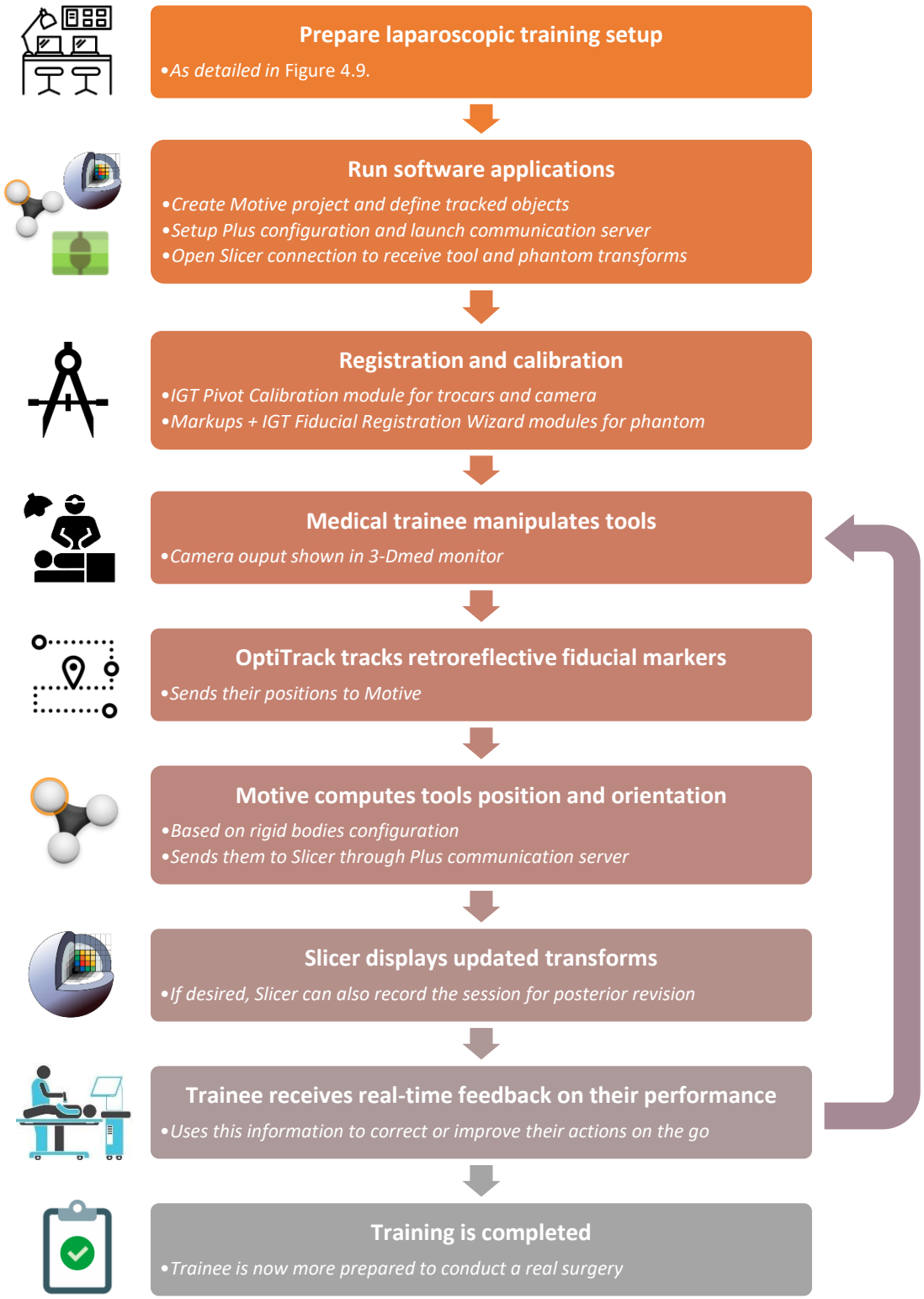

Figure 4.15. General flowchart of the development of an image-guided laparoscopic training session.

5. *Results and Discussion*

Every component of the full-scale phantom fits together seamlessly, and the training software effectively allows real-time navigation of the phantom.

5.1. Production of the torso

The torso was 3D-printed in three parts –thorax, pelvis, and breast plate– to enable modular application if desired. The FDM printing technique with PLA polyester material provided a durable, reasonably priced, light-weighted, and sufficiently accurate result. Still, the price was slightly higher than expected, but the reason for this was a mistake in the communication with the external printing company (Sicnova 3D, Madrid).

As previously mentioned, the chest plate had to be reconstructed by boolean operations, due to errors in the OpenHELP dataset [49]. It perfectly fitted with the upper torso, as evidenced in *Figure 4.1* and *Figure 4.3*.

Significant defects were realized in the upper torso print, detailed in *Figure 5.1*. These were caused by a minor miscalibration of the FDM printer of the external company. However, the protuberances were easily chopped off with a cutter knife, causing no trouble when fitting the chest plate.

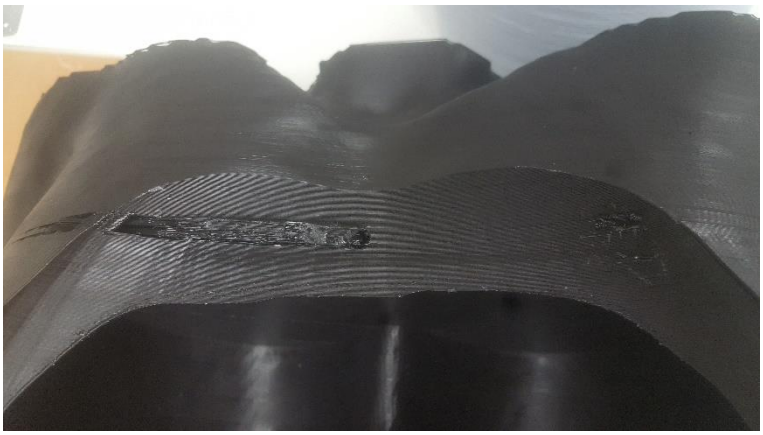

Figure 5.1. Printing defects found in the upper torso of the phantom.

5.2. Production of the organs

5.2.1. Modelling and printing of organ molds

Molds were generated based on the digital models of the organs, and printed with the same FDM method as for the torso. For the molds, the 3D printer Ultimaker 3 Extended at our university was employed; the advantages of this were cheaper costs (only the material and printer expenses were incurred) and flexibility for materialization of the molds in separate batches. However, the use of the printer was subject to availability and printing time constraints, which occasionally slowed down the process.

The first design of the molds was not based on extrusion of the organs, but rather it consisted on cuboids surrounding the surface of the organs, a design that was needlessly more material-intensive. *Figure 5.2* illustrates the printing of these designs, together with several printing defects originated from major miscalibrations of the 3D printer.

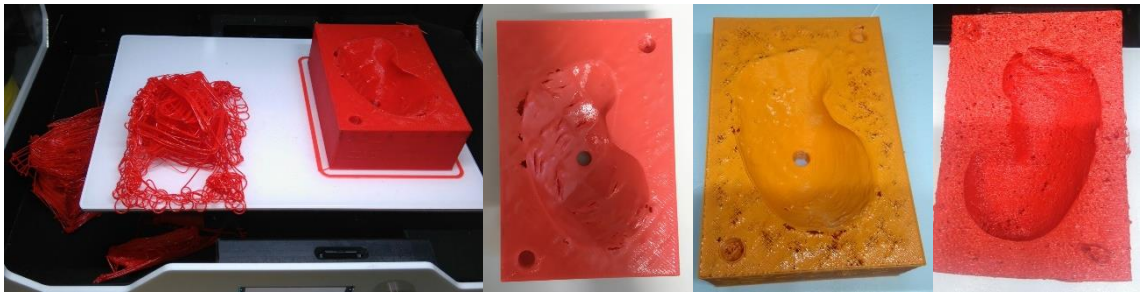

Figure 5.2. Printing errors on the initial version of the organ molds, including warping, detachment of the first layer, under-extrusion and pillowing.

On the other side, the final version of the molds is shown in *Figure 5.3*. The accuracy of these prints was satisfactory, although the alignment between junctions of geometrically complex molds was not perfect, which would be detrimental for the next step of mold casting.

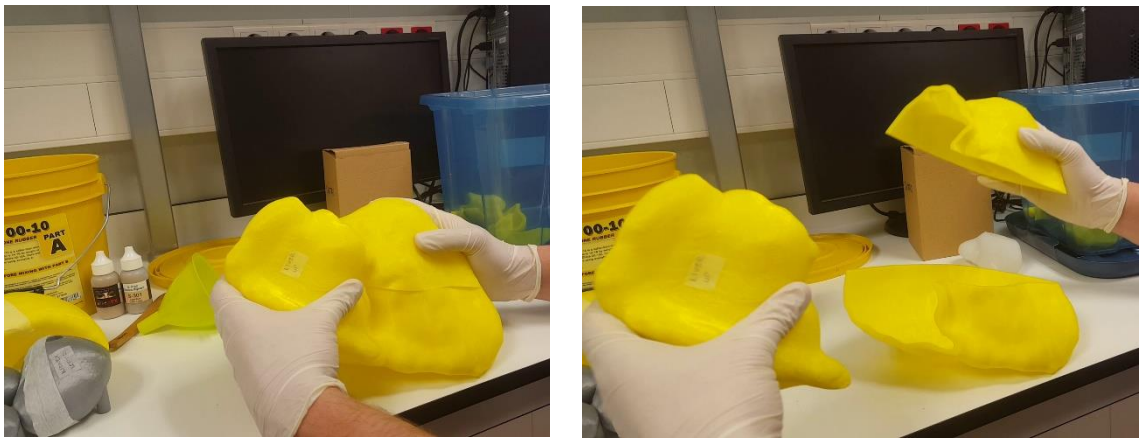

Figure 5.3. Liver mold is illustratively shown, with its constituent parts joined (left) and separated (right).

5.2.2. Mold casting and production of organs

Silicone casting of the organs was conducted with moderate complications. As it has been said in section *5.2.1*, the most complex molds were not perfectly accurate, so the misalignment between parts occasioned leaking of silicone. In some molds, it was difficult to attach the different pieces, which also contributed to silicone leakages. Various methods were tested, such as using modelling clay or adhesive tape, but this last one proved to be the most effective. Glue would have been optimal in terms of fluid-tightness, but since the parts needed to be separated after silicone curation, it was not a feasible approach.

In some cases, the process of filling the molds had to be repeated to compensate for leakages, pouring new silicone over the already cured one. However, no differences or defects were noticed between overlapping castings, and all the organs ended up having a solid consistency and a smooth surface. *Figure 5.4* shows the whole set of silicone organs inside the 3D-printed torso.

Figure 5.4. Silicone organs placed inside the torso with the breast shield (left), and without it (right).

5.3. Production of the abdominal cover

A realistic artificial skin was created for the abdominal aperture of the phantom. It was comprised of a 3D-printed framework and an EVA foam sheet. The structural base was designed with a grating pattern, far more efficient regarding printing time and material than a solid infill. The grating design also facilitated piercing holes in the EVA sheet through which laparoscopic tools could be inserted, as illustrated in *Figure 5.5*.

Figure 5.5. Detail of the anterior (left) and posterior (right) sides of the abdominal artificial skin.

5.4. Preparation of the tracking system

Five rigid body structures were created with distinct angle configurations, which hosted three fiducial markers (retroreflective infrared spheres) each. Three of these five rigid bodies were attached through specially designed coupling parts to the two trocars and the laparoscopic camera, as shown in *Figure 4.13*. Another rigid body was simply adhered to the phantom with adhesive tape.

The navigation tools were manually modeled (see *Figure 4.12*) after unsuccessful attempts of performing 3D surface scans on them. A link to these and all the other 3D models of the project can be found in Annexes for online download.

5.5. Validation of the phantom and navigation system

The complete navigation system proved to be an asset for training of laparoscopic and image-guided procedures. Two members of the bioengineering department assessed the perceived level of realism and accuracy (*Figure 5.6*), one of which was recorded both in video and in Slicer. Links to these files can be found in *Annex I*, while *Annex I.*

The results revealed that the general feeling of immersion was accomplished, with minor flaws in calibration that caused occasional overlapping of models in the Slicer scene, as

evidenced in *Figure 5.7*. The overall evaluation was favorable despite the imperfections in calibration, which were explained by three reasons: (i) minimal differences between modelled and real navigation tools; (ii) unstable attachment of the docking pieces to the laparoscopic tools; and (iii) slight curvature in the elongated, supposedly straight parts of the tools. Altogether, these incidents contributed to small deviations of the tracked markers positions with respect to the tips of their respective tools.

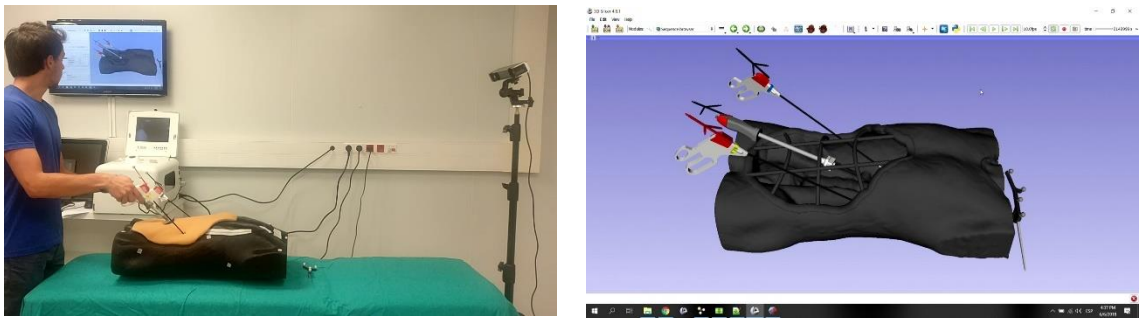

Figure 5.6. Evaluation of the image-guided laparoscopic training system (left), with detail of the computer screen running Slicer for real-time navigation (right).

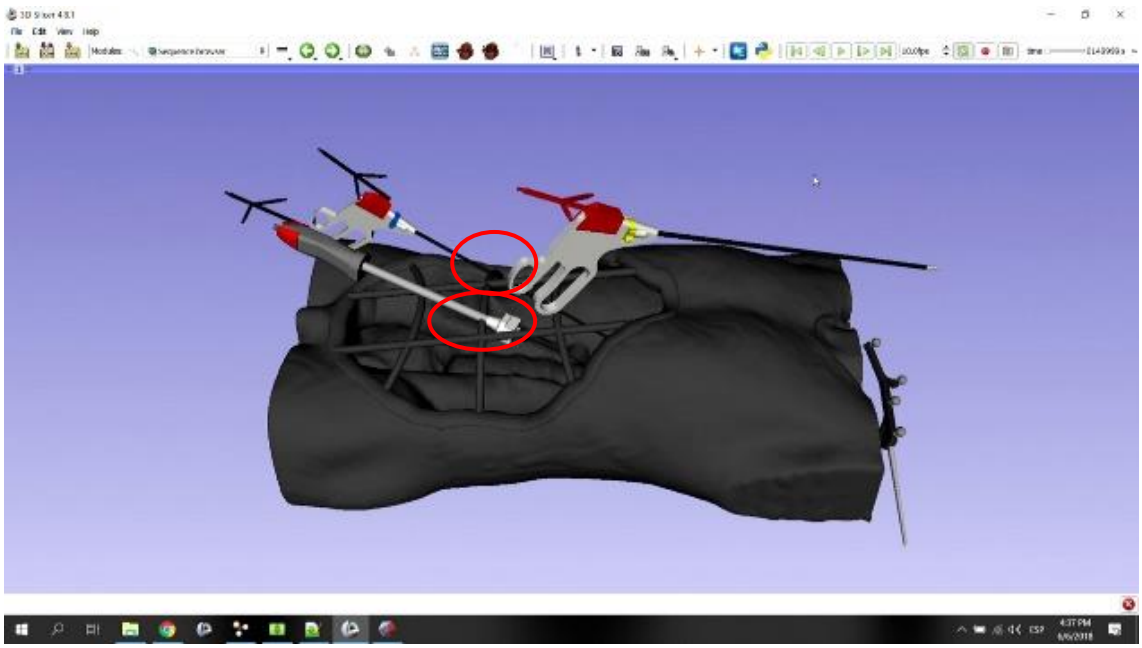

Figure 5.7. Calibration flaws that occasionally caused overlapping of digital models in Slicer.

6. Conclusions

In this project, a realistic system for image-guided laparoscopic training was built, consisting of two main components: (1) a reusable, easily reproducible phantom model with accurate anatomical features, and (2) an image-guided laparoscopic surgery setup, including an optical tracking system, and the use of specific software to navigate the phantom in real time, and to record the activity of the trainee for posterior analysis of performance.

For the phantom, every anatomical structure could be correlated to their counterparts in a real human body. However, as it was mentioned in section *4.3.1*, the organs of the mediastinum were lacking because their molds could not be printed in time. This was due to material and time constraints of the 3D printer of the bioengineering department, which had to be shared simultaneously between multiple projects.

It should be noted that our needs were particularly intensive in terms of printing time and material though, with 38 different prints required only for the molds, which accounted for a total of approximately 420 hours. Since the design of the organ molds was conceived to use minimum amounts of material, the only possible workaround would have been ordering the printing to an external company, as with the torso.

The attachment between component parts of the molds was problematic. It could have been improved with the addition of structures that guaranteed the pieces stayed fixed to each other during the casting process, saving both silicone and time in the process.

It could have also been improved changing the way in which molds were segmented to divide them in separable parts. Silicone leaks were observed to happen almost exclusively around sharp edges of junctions between parts, probably because of limitations in the resolution of the 3D printer. In view of this, perhaps it could be solved by changing the plane cuts performed on the molds by round ones, or at least use more organic shapes for slicing.

Silicone organs were produced with moderate difficulties. The union between parts of the molds was unstable, and sometimes it caused major silicone leaks. Despite the complications in the production process, the end results were consistent, resistant organs with a smooth surface.

An artificial skin cover was created for the abdominal area of the phantom, composed of a 3D-printed framework and an EVA foam sheet. The first was designed with a hollow grating-pattern, which proved to be optimal for achieving light weight and minimum printing times and material without compromising resistance and functionality. The EVA sheet also provided an inexpensive, realistic solution for emulating the abdominal skin.

Five tracking markers were created with different angular configurations, so that each could be recognizable to the motion capture software. Only four of these five markers were finally employed, one for tracking the phantom, and the other three for the navigation tools: two trocars, identical to those used in minimally invasive surgeries, and a laparoscopy camera, part of the 3-Dmed laparoscopy simulator. A pointer stylus was also used for precise registration and calibration of the system, but it already had four fiducial markers incorporated on it, so a tracking marker was not needed in this case.

Unfortunately, the disposition of three of the fiducial markers in the pointer stylus closely resembled the configuration of one of the rigid bodies (the corresponding to the right trocar), as illustrated in *Figure 6.1*. This could have caused sporadic interferences in the tracking of both tools; yet, the pointer was only used for registration and calibration of the system, prior to the actual navigation stage. Hence, in the end it did not become an obstacle, but it could still have been easily prevented by replacing the problematic rigid body for the extra, unused one.

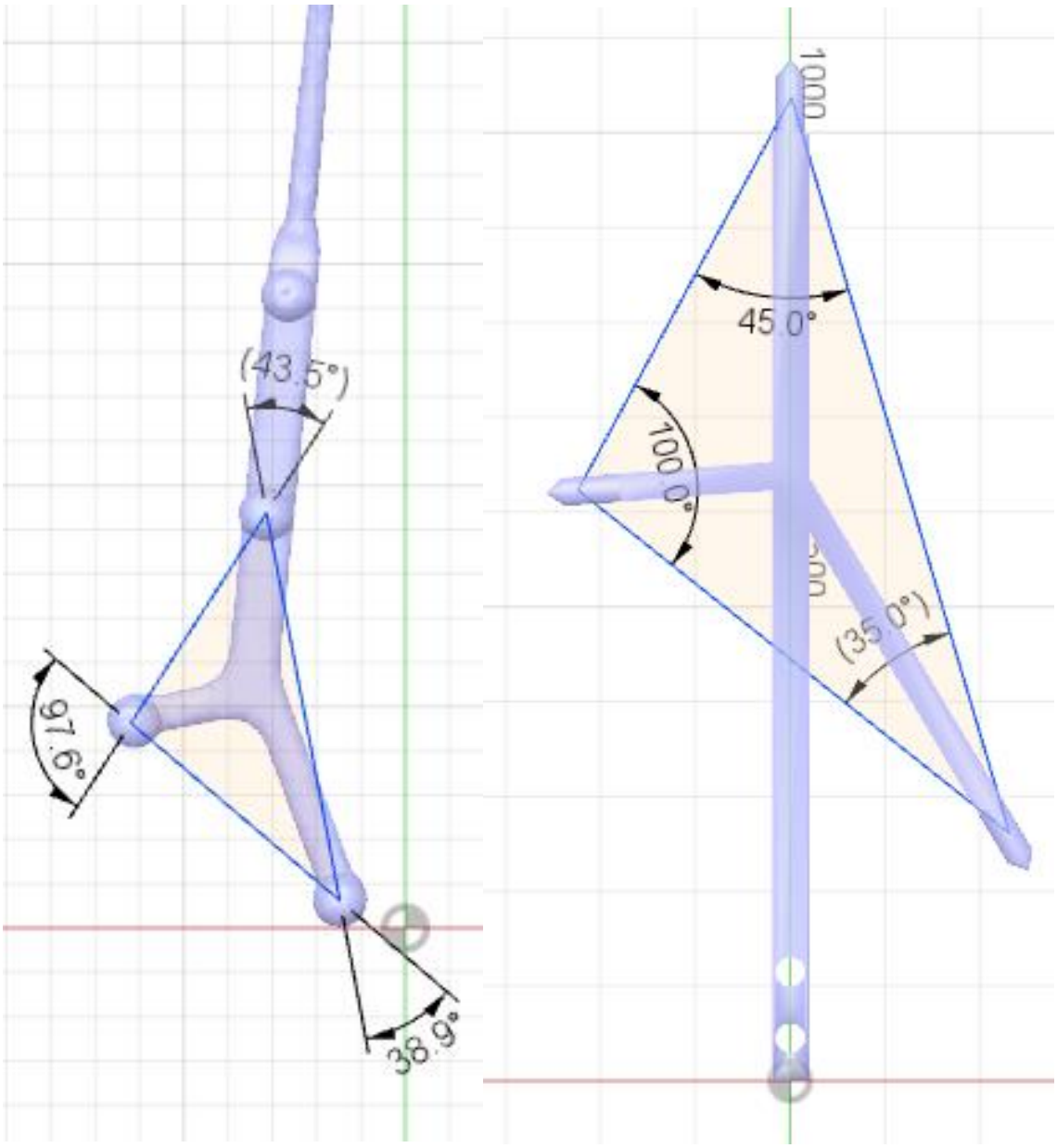

Figure 6.1. Comparison between angle configurations of the pointer stylus (left) and the right trocar rigid body (right).

Once finished, an evaluation of the complete system was conducted by testing it with two members of the bioengineering department, which returned favorable results. The training software effectively allowed real time navigation of the phantom and recorded the activity of one participant, which could be later used for revision and performance analysis.

From the 4,700€ total cost, the torso made up for most of the expenses. Fortunately, they were nonrecurring costs because the plastic torso was very durable. Also, we deemed that we had been slightly overcharged for this order by the external company.

When compared to similar projects, our solution was one of the most inexpensive. The closest could be the OpenHELP phantom, whose budget was of 5,800€. This disparity originated mainly from the 3D printing techniques chosen for materialization of the torso –500€ difference– and the organ molds –300€–, as summarized in *Table 4.1*. They used SLS for the torso and gypsum 3D printing for the organs, which usually produce less economical, but moderately higher quality results than our FDM technique. Still, the end quality of our phantom was completely satisfactory.

7. Future Work

Two members of the bioengineering department assessed the perceived level of accuracy and immersion of the laparoscopic training system. However, the nature of these tests was rather subjective. It remained to perform some test on the phantom with a more objective evaluation criterion, such as evaluation of haptic realism in a defined scale, or measuring the reproduction accuracy with statistical features, like the root-mean-square deviation.

Also, a larger test group could be formed in the future, preferably composed by experienced medical students or surgeons. Likewise, the software should be further developed to better assess the evolution of participants thanks to our training system, extracting measurements that enable an exhaustive analysis of user performance.

Another important future improvement would be related to the user interface of Slicer, which is quite intricate and may confuse the user amongst the numerous modules and options available. It would be very practical to develop one single module that combined all the functionalities required for our project. This thorough module would merge functions from at least the IGT, Sequences, Data, Models and Markups modules.

Finally, it was realized that the laparoscopy camera lacked a light source for illumination of the dim interior of the phantom; for next applications, a small one should be attached to the tip of the camera.

8. Project Socio-economic Impact

8.1. Project Budget

The following is a breakdown of the different expenses incurred during the project. They are divided into direct and equipment costs, accounting for a global total of 22,045€.

8.1.1. Direct expenses

Table 8.1. Direct costs of the project.

Concept	*Unitary cost*	*Amount*	*Total cost*
Torso printing (3 elements)	20 €/h	200 hours	**4,000 €**
Organ molds printing (18 elements)	31 €/kg	1.79 kg	**55 €**
Abdominal plate printing (6 elements)	31 €/kg	0.20 kg	**6 €**
Ecoflex 00-10	30 €/kg	7 kg	**210 €**
Ecoflex 00-30	30 €/kg	14 kg	**420 €**
FFX S-301 Light	26 €/30g	15 g	**13 €**
Artificial skin EVA sheets	1 €/unit	10 units	**10 €**
Student salary	15 €/h	450 hours	**6,750 €**
Tutor salary	25 €/h	400 hours	**10,000 €**
TOTAL			**21,465 €**

As for the printing of the organ molds, below is a detailed list of each individual expense, including also printing errors and cancelled prints. The calculations were done with the printer's own software, Ultimaker Cura.

Table 8.2. Breakdown of organ molds printing costs.

Print order	*Print time*	*Material amounts*	*Total cost*
Duodenum (4 parts)	10.2 h	39 g PLA + 14 g PVA	**2.50 €**
Stomach (3 parts)	27.5 h	118 g PLA + 60 g PVA	**9.60 €**

Liver (3 parts)	61.5 h	423 g PLA	**10 €**
Spleen (2 parts)	28.3 h	159 g PLA + 25 g PVA	**6.60 €**
Pancreas (5 parts)	15.4 h	98 g PLA	**2.30 €**
Rectum Lumen (2 parts)	45.5 h	175 g PLA	**4.20 €**
Pelvic Muscles (3 parts)	53.3 h	201 g PLA	**4.80 €**
Bladder (2 parts)	17.2 h	86 g PLA + 39 g PVA	**6.50 €**
Kidney Left (2 parts)	8.1 h	89 g PLA	**2.10€**
Kidney Right (2 parts)	7.9 h	86 g PLA	**2 €**
Failed prints (7 occurrences)	36.5 h *(total)*	175 g PLA + 7 g PVA	**4.90 €**

8.1.2. Equipment Costs

Table 8.3. Equipment costs of the project.

Concept	*Cost*	*Depreciation*	*Dedication*	*Total cost*
Silicone manipulation tools	25 €	-	-	**25 €**
Computer usage	800 €	20% per year	100% for 1 year	**160 €**
3D printer usage	4,500 €	33% per year	50% for 6 months	**375 €**
OptiTrack Duo usage	2,000 €	20% per year	100% for 2 weeks	**17 €**
3-Dmed T9 series usage	2,500 €	20% per year	100% for 2 days	**3 €**
TOTAL				**580 €**

8.2. Social Impact

The bioengineering department at University Carlos III of Madrid is constantly testing new devices and approaches to improve image-guided surgery. This laparoscopic training system will be a valuable resource for many research projects of the department.

One example could be a current project aimed at developing an augmented reality (AR) software application which uses the AR glasses HoloLens, and the software development kits Unity and Vuforia. Based on a cubical 3D marker, it recognizes the surroundings and performs several actions, such as superposing digital models on top of its real

counterparts. Our phantom could be the perfect host for this application, for instance, by placing data or digital models of organs, surgical guides, or tools in relation to the realistic disposition of silicone organs in the interior of the phantom. An illustration of this possibility is shown in *Figure 8.1*.

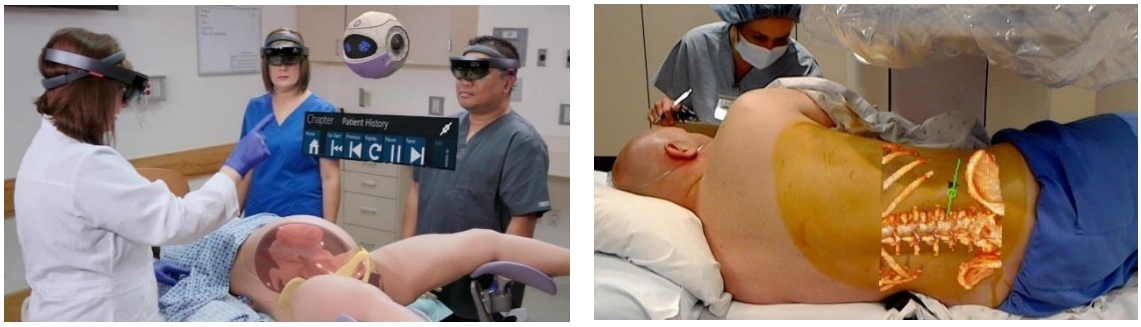

Figure 8.1. Examples of augmented reality possible applications in gynaecological (left) and spine (right) surgeries [78, 79].

Other uses for our project would include collaboration with our partner institution, the General University Hospital Gregorio Marañón. After polishing some details to improve the level of realism, the system could be used for what it has been designed: training of laparoscopy and image-guided surgery skills of medical students. It has been reported that the use of this kind of phantoms is practical, and highly beneficial to make the students feel more prepared towards performing a real surgery.

9. Annexes

9.1. Annex I

Link to folder containing all digital 3D models, including the torso, organs, molds, rigid bodies and navigation tools: goo.gl/MSrUca

9.2. Annex II

Figure 9.1. Video recording of tools calibration before project evaluation.

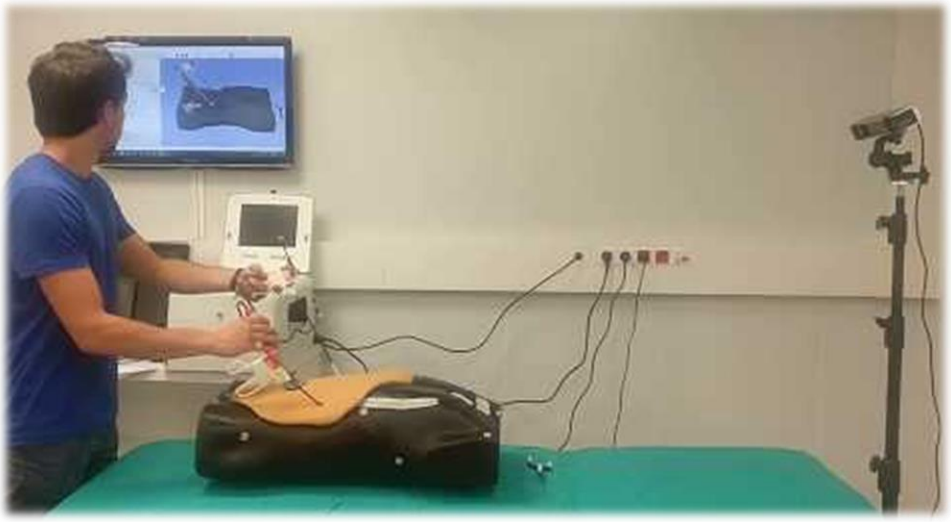

Figure 9.2. Video recording of project evaluation.

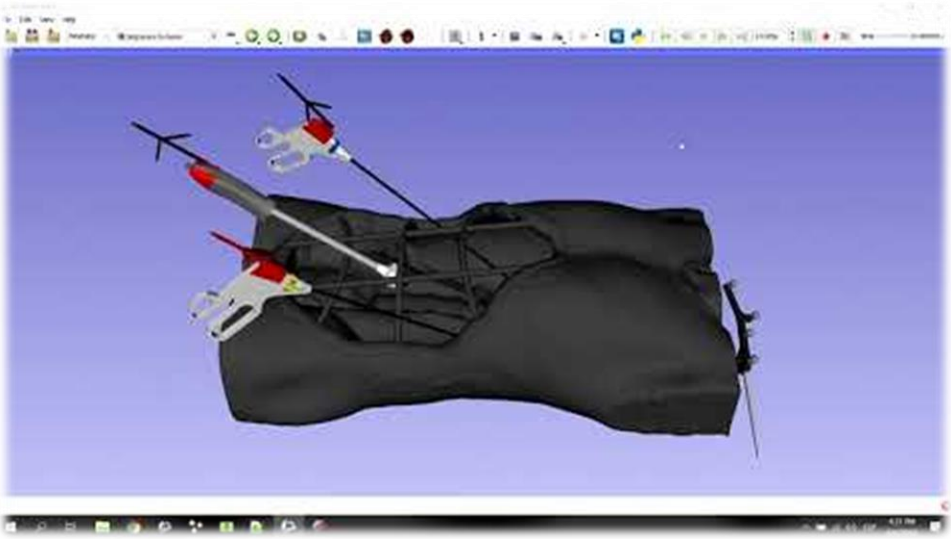

Figure 9.3. Screencast of Slicer during project evaluation.

10. Bibliography

[1] A. Buia, F. Stockhausen and E. Hanisch, "Laparoscopic surgery: A qualified systematic review," *World Journal of Methodology*, vol. 5, no. 4, pp. 238-254, 2015.

[2] VectorStock, "Schematic laparoscopic surgery vector image," [Online]. Available: https://www.vectorstock.com/royalty-free-vector/schematic-laparoscopic-surgery-vector-801492. [Accessed 2018].

[3] J. W. Milsom and B. Böhm, "Advantages and Disadvantages of Laparoscopic Colorectal Surgery," *Laparoscopic Colorectal Surgery*, pp. 225-231, 1996.

[4] S. Krishnakumar and P. Tambe, "Entry Complications in Laparoscopic Surgery," *Journal of Gynecological Endoscopy and Surgery*, vol. 1, no. 1, pp. 4-11, 2009.

[5] J. De Loose and S. Weyers, "A laparoscopic training model for surgical trainees," *Gynecological Surgery*, vol. 14, no. 1, p. 24, 2017.

[6] Simulab, "Universal Surgical Abdomen Team Training System," [Online]. Available: https://www.simulab.com/products/traumaman-system/traumaman-surgical-abdomen-team-training-system. [Accessed 2018].

[7] Imaging Solutions, "TraumaMan Surgical Abdomen Team Training System," [Online]. Available: https://www.imagingsol.com.au/product/1811/CT-Torso-Phantom-CTU-41.html. [Accessed 2018].

[8] G. M. Fried, A. M. Derossis, J. Bothwell and H. H. Sigman, "Comparison of laparoscopic performance in vivo with performance measured in a laparoscopic simulator," *Surgical Endoscopy*, vol. 13, no. 11, pp. 1077-1081, 1999.

[9] K.-H. Ng and C.-H. Yeong, "Imaging Phantoms: Conventional X-ray Imaging Applications," in *The Phantoms of Medical and Health Physics*, Madison, Springer, 2014, pp. 91-122.

[10] N. Din, P. Smith, K. Emeriewen, A. Sharma, S. Jones, J. Wawrzynski, H. Tang, P. Sullivan, S. Caputo and G. M. Saleh, "Man versus Machine: Software Training for

Surgeons—An Objective Evaluation of Human and Computer-Based Training Tools for Cataract Surgical Performance," *Journal of Ophthalmology*, vol. 2016, pp. 1-7, 2016.

[11] H. Maertens, A. Madani, T. Landry, F. Vermassen, I. Van Herzeele and R. Aggarwal, "Systematic review of e-learning for surgical training.," *British Journal of Surgery*, vol. 103, no. 11, pp. 1428-1437, 2016.

[12] J. Bric, M. Connolly, A. Kastenmeier, M. Goldblatt and J. Gould, "Proficiency training on a virtual reality robotic surgical skills curriculum.," *Surgical Endoscopy*, vol. 28, no. 12, pp. 3343-3348, 2014.

[13] engineering.com, "3D Systems Medical Goes Virtual with VR OR Surgical Training," [Online]. Available: https://www.engineering.com/3DPrinting/3DPrintingArticles/ArticleID/14190/3D-Systems-Medical-Goes-Virtual-with-VR-OR-Surgical-Training.aspx. [Accessed 2018].

[14] AppReal, "Virtual Reality Surgery: The Future of Healthcare," [Online]. Available: https://appreal-vr.com/blog/understanding-vr-surgery/. [Accessed 2018].

[15] M. P. Fried, R. Satava, S. Weghorst, A. Gallagher, C. Sasaki, D. Ross, M. Sinanan, H. Cuellar, J. I. Uribe, M. Zeltsan and H. Arora, "The Use of Surgical Simulators to Reduce Errors," in *Advances in Patient Safety: From Research to Implementation (Volume 4: Programs, Tools, and Products).*, Rockville, Agency for Healthcare Research and Quality, 2005.

[16] J. Røtnes, J. Kaasa, G. Westgaard, E. Eriksen, P. Hvidsten, K. Strøm, V. Sørhus, Y. Halbwachs, E. Haug, M. Grimnes, H. Fontenelle, T. Ekeberg, J. Thomassen, O. Elle and E. Fosse, "A tutorial platform suitable for surgical simulator training (SimMentor).," *Studies in Health Technology and Informatics*, vol. 85, pp. 419-425, 2002.

[17] K. G. Vosburgh, "Image Guided Surgery and Its Potential," *Studies in Health Technology and Informatics*, vol. 39, pp. 83-89, 1997.

[18] Brainlab.org, "What is Software-Guided Surgery for Knee?," [Online]. Available: https://www.brainlab.org/get-educated/knee/understand-software-guided-surgery-for-knee/what-is-software-guided-surgery-for-knee/. [Accessed 2018].

[19] P. Sánchez-González, A. M. Cano, I. Oropesa, F. M. Sánchez-Margallo, F. D. Pozo, P. Lamata and E. J. Gómez, "Laparoscopic video analysis for training and image-guided surgery," *Minimally Invasive Therapy & Allied Technologies,* vol. 20, no. 6, pp. 311-320, 2011.

[20] 24x7 Magazine, "FDA Clears 7D Surgical's Image Guidance System for Spine Surgery," [Online]. Available: http://www.24x7mag.com/2017/01/fda-clears-7d-surgicals-image-guidance-system-spine-surgery/. [Accessed 2018].

[21] Cosas de Arquitectos, "Impresión 3D por compactación o solidificación de materiales," [Online]. Available: http://www.cosasdearquitectos.com/2014/04/impresion-3d-por-compactacion-de-o-solidificacion-de-materiales/. [Accessed 2018].

[22] MKS Technologies Pvt Ltd., "Stereolithography (SLA)," [Online]. Available: http://www.mkstechgroup.com/stereolithography-sla/. [Accessed 2018].

[23] Potomac, "3D Printed Microfluidic Device," [Online]. Available: https://www.potomac-laser.com/project-gallery/3d-printed-microfluidic-device/. [Accessed 2018].

[24] 24horas, "Padre fabrica prótesis para su hijo con una impresora 3D," [Online]. Available: http://www.24horas.cl/tendencias/salud-bienestar/padre-fabrica-protesis-para-su-hijo-con-una-impresora-3d-948928. [Accessed 2018].

[25] Homeli, "Exo 3D Printed Prosthetic Limbs by William Root," [Online]. Available: http://homeli.co.uk/exo-3d-printed-prosthetic-limbs-by-william-root/. [Accessed 2018].

[26] NIH Director's Blog, "Building a Better Scaffold for 3D Bioprinting," [Online]. Available: https://directorsblog.nih.gov/2015/11/03/building-a-better-scaffold-for-3d-bioprinting/. [Accessed 2018].

[27] M. S. Wróbel, M. Jędrzejewska-Szczerska, S. Galla, L. Piechowski, M. Sawczak, A. P. Popov, A. V. Bykov, V. V. Tuchin and A. Cenian, "Use of optical skin phantoms for preclinical evaluation of laser efficiency for skin lesion therapy," *Journal of Biomedical Optics,* vol. 20, no. 8, 2015.

[28] S. E. Bohndiek, S. Bodapati, D. V. D. Sompel, S.-R. Kothapalli and S. S. Gambhir, "Development and Application of Stable Phantoms for the Evaluation of Photoacoustic Imaging Instruments," *PLOS One,* vol. 8, no. 9, 2013.

[29] B. N. Rome, D. B. Kramer and A. S. Kesselheim, "Approval of High-Risk Medical Devices in the US: Implications for Clinical Cardiology," *Current Cardiology Reports,* vol. 16, no. 6, p. 489, 2014.

[30] Ultrasound Schools Info, "Ultrasound Technician Internships," [Online]. Available: https://www.ultrasoundschoolsinfo.com/internships/. [Accessed 2018].

[31] Veterinary Care Specialists, "Veterinary Ultrasound," [Online]. Available: http://www.vcsmilford.com/Services/Ultrasound.aspx. [Accessed 2018].

[32] GT Simulators, "Ultrasound Examination Training Model - ABDFAN," [Online]. Available: https://www.gtsimulators.com/Ultrasound-Examination-Training-Model-ABDFAN-p/kkus-1b.htm. [Accessed 2018].

[33] B. Böhm and J. W. Milsom, "Animal models as educational tools in laparoscopic colorectal surgery," *Surgical Endoscopy,* vol. 8, no. 6, pp. 707-713, 1994.

[34] M. A. Pereira-Sampaio, L. A. Favorito and F. J. Sampaio, "Pig kidney: anatomical relationships between the intrarenal arteries and the kidney collecting system. Applied study for urological research and surgical training.," *The Journal of Urology,* vol. 172, no. 5, pp. 2077-2081, 2004.

[35] H. G. Kenngott, J. J. Wünscher, M. Wagner, A. Preukschas, A. L. Wekerle, P. Neher, S. Suwelack, S. Speidel, F. Nickel, D. Oladokun, L. Maier-Hein, R. Dillmann, H. P. Meinzer and B. P. Müller-Stich, "OpenHELP (Heidelberg laparoscopy phantom): development of an open-source surgical evaluation and training tool," *Surgical Endoscopy,* vol. 29, no. 11, pp. 3338-3347, 2015.

[36] L. A. DeWerd and M. Lawless, "Introduction to Phantoms of Medical and Health Physics," in *The Phantoms of Medical and Health Physics*, Nueva York, Springer-Verlag, 2014, pp. 1-14.

[37] Laerdal, "Resusci Anne QCPR," [Online]. Available: https://www.laerdal.com/fr/products/simulation-training/resuscitation-training/resusci-anne-qcpr/. [Accessed 2018].

[38] X. G. Xu, "An exponential growth of computational phantom research in radiation protection, imaging, and radiotherapy: A review of the fifty-year history," *Physics in Medicine and Biology,* vol. 59, no. 18, pp. 233-302, 2014.

[39] K. E. Keenan, L. J. Wilmes, S. O. Aliu, D. C. Newitt, E. F. Jones, M. A. Boss, K. F. Stupic, S. E. Russek and N. M. Hylton, "Design of a breast phantom for quantitative MRI," *Journal of Magnetic Resonance Imaging,* vol. 44, no. 3, pp. 610-619, 2016.

[40] K. Keenan, A. Peskin, L. Wilmes, S. Aliu, E. Jones, W. Li, J. Kornak, D. Newitt and N. Hylton, "Variability and bias assessment in breast ADC measurement across multiple systems.," *Journal of Magnetic Resonance Imaging,* vol. 44, no. 4, pp. 846-855, 2016.

[41] Kyoto Kagaku, "Dynamic Heart and Lung Phantom," [Online]. Available: https://www.kyotokagaku.com/products/detail03/ph-48.html. [Accessed 2018].

[42] C. Hsieh, G. Gladish and C. E. Willis, "Evaluation of a commercial cardiac motion phantom for dual-energy chest radiography," *Journal of Applied Clinical Medical Physics,* vol. 15, no. 2, pp. 235-251, 2014.

[43] W. D. M. A. F. A. D. E. S. A. v. D. S. F. H. F. H. Gillen S, "The "ELITE" model: construct validation of a new training system for natural orifice transluminal endoscopic surgery (NOTES).," *Endoscopy,* vol. 41, no. 5, pp. 395-399, 2009.

[44] G. Sankaranarayanan, K. Matthes, A. Nemani, W. Ahn, M. Kato, D. B. Jones, S. Schwaitzberg and S. De, "Needs analysis for developing a virtual-reality NOTES simulator.," *Surgical Endoscopy,* vol. 27, no. 5, pp. 1607-1616, 2013.

[45] A. Nemani, G. Sankaranarayanan, J. S. Olasky, S. Adra, K. E. Roberts, L. Panait, S. D. Schwaitzberg, D. B. Jones and S. De, "A comparison of NOTES transvaginal and laparoscopic cholecystectomy procedures based upon task analysis.," *Surgical Endoscopy*, vol. 28, no. 8, pp. 2443-2451, 2014.

[46] GT Simulators, "Fast/Acute Abdomen Phantom," [Online]. Available: https://www.gtsimulators.com/Fast-Acute-Abdomen-Phantom-FAST-ER-FAN-p/kkus-5.htm. [Accessed 2018].

[47] GT Simulators, "X-Ray Phantom Spine Model," [Online]. Available: https://www.gtsimulators.com/X-Ray-Phantom-Transparent-Spine-Model-p/ez7290.htm. [Accessed 2018].

[48] VirtaMed, "Custom simulators using original surgical devices," [Online]. Available: https://www.virtamed.com/en/custom-made-simulators/customized-simulators/. [Accessed 2018].

[49] Open-CAS, "OpenHELP (Heidelberg laparoscopy phantom)," [Online]. Available: http://opencas.webarchiv.kit.edu/?q=node/27. [Accessed 2018].

[50] S. Müller, A. Bihlmaier, S. Irgenfried and H. Wörn, "Hybrid Rendering Architecture for Realtime and Photorealistic Simulation of Robot-Assisted Surgery," *Studies in Health Technology and Informatics*, vol. 220, pp. 245-250, 2016.

[51] M. Wagner, M. Gondan, C. Zöllner, J. J. Wünscher, F. Nickel, L. Albala, A. Groch, S. Suwelack, S. Speidel, L. Maier-Hein, B. P. Müller-Stich and H. G. Kenngott, "Electromagnetic organ tracking allows for real-time compensation of tissue shift in image-guided laparoscopic rectal surgery: results of a phantom study," *Surgical Endoscopy*, vol. 30, no. 2, pp. 495-503, 2016.

[52] R. Galloway and T. Peters, "Overview and History of Image-Guided Interventions," in *Image-Guided Interventions*, Boston, Springer, 2008, pp. 1-21.

[53] K. Cleary and T. Peters, "Image-guided interventions: technology review and clinical applications," *Annual Review of Biomedical Engineering*, vol. 12, no. 1, pp. 119-142, 2010.

[54] J. West and C. J. Maurer, "Designing optically tracked instruments for image-guided surgery," *IEEE Transactions on Medical Imaging*, vol. 23, no. 5, pp. 533-545, 2004.

[55] K. Mekuria, Y. Kim, H. Cho, D. Lee, S. Park, B. H. Lee, K.-M. Jang and J. H. Wang, "The Effect of Optical Marker Configuration on Tracking Accuracy in Image Guided Surgery," *Studies in Health Technology and Informatics*, vol. 220, pp. 227-232, 2016.

[56] Z. Yaniv and E. Wilson, "Electromagnetic tracking in the clinical environment," *Medical Physics*, vol. 36, no. 3, pp. 876-892, 2009.

[57] H. Zhang, F. Banovac, R. Lin, N. Glossop, B. J. Wood, D. Lindisch, E. Levy and K. Cleary, "Electromagnetic tracking for abdominal interventions in computer aided surgery," *Computer Assisted Surgery*, vol. 11, no. 3, pp. 127-136, 2006.

[58] Chae, YS, S. Lee, H. Lee and M. Kim, "Optical coordinate tracking system using afocal optics for image-guided surgery," *International Journal of Computer Assisted Radiology and Surgery*, vol. 10, no. 2, pp. 231-241, 2015.

[59] J. D. Bric, D. C. Lumbard, M. J. Frelich and J. C. Gould, "Current state of virtual reality simulation in robotic surgery training: a review," *Surgical Endoscopy*, vol. 30, no. 6, pp. 2169-2178, 2016.

[60] D. Zerbato and D. Dall'Alba, "Role of virtual simulation in surgical training," *Journal of Visualized Surgery*, vol. 3, p. 23, 2017.

[61] D. C. Gray, E. M. Kim, V. E. Cotero, A. Bajaj, V. P. Staudinger, C. A. Tan Hehir and S. Yazdanfar, "Dual-mode laparoscopic fluorescence image-guided surgery using a single camera," *Biomedical Optics Express*, vol. 3, no. 8, pp. 1880-1890, 2012.

[62] M. Wagner, M. Gondan, C. Zöllner, J. Wünscher, F. Nickel, L. Albala, A. Groch, S. Suwelack, S. Speidel, L. Maier-Hein, B. Müller-Stich and H. Kenngott, "Electromagnetic organ tracking allows for real-time compensation of tissue shift

in image-guided laparoscopic rectal surgery: results of a phantom study," *Surgical Endoscopy,* vol. 30, no. 2, pp. 495-503, 2016.

[63] H. Dodziuk, "Applications of 3D printing in healthcare," *Polish Journal of Cardio-Thoracic Surgery,* vol. 13, no. 3, pp. 283-293, 2016.

[64] C. L. Ventola, "Medical Applications for 3D Printing: Current and Projected Uses," *P & T : a peer-reviewed journal for formulary management,* vol. 39, no. 10, pp. 704-711, 2014.

[65] L. E. Diment, M. S. Thompson and J. H. M. Bergmann, "Clinical efficacy and effectiveness of 3D printing: a systematic review," *BMJ Open,* vol. 7, no. 12, 2017.

[66] C. Hazelaar, M. van Eijnatten, M. Dahele, J. Wolff, T. Forouzanfar, B. Slotman and W. Verbakel, "Using 3D printing techniques to create an anthropomorphic thorax phantom for medical imaging purposes," *Medical Physics,* vol. 45, no. 1, pp. 92-100, 2018.

[67] A. J. Cloonan, D. Shahmirzadi, R. X. Li, B. J. Doyle, E. E. Konofagou and T. M. McGloughlin, "3D-Printed Tissue-Mimicking Phantoms for Medical Imaging and Computational Validation Applications," *3D Printing and Additive Manufacturing,* vol. 1, no. 1, pp. 14-23, 2014.

[68] National Institutes of Health, "About the NIH 3D Print Exchange," [Online]. Available: https://3dprint.nih.gov/about. [Accessed 2018].

[69] J. Garcia, Z. Yang, R. Mongrain, R. L. Leask and K. Lachapelle, "3D printing materials and their use in medical education: a review of current technology and trends for the future," *BMJ Simulation & Technology Enhanced Learning,* vol. 4, no. 1, pp. 27-40, 2018.

[70] T. J. Horn and O. L. A. Harrysson, "Overview of current additive manufacturing technologies and selected applications," *Science Progress,* vol. 95, no. 3, pp. 255-282, 2012.

[71] X. Pang, X. Zhuang, Z. Tang and X. Chen, "Polylactic acid (PLA): research, development and industrialization," *Biotechnology Journal,* vol. 5, no. 11, pp. 1125-1136, 2010.

[72] S. R. Bathula, Virupakshi and H. Mali, "3D Printing for Foot," *MOJ Proteomics & Bioinformatics,* vol. 5, no. 6, 2017.

[73] C. Duran, V. Subbian, M. T. Giovanetti, J. R. Simkins and F. Beyette, "Experimental desktop 3D printing using dual extrusion and water-soluble polyvinyl alcohol," *Rapid Prototyping Journal,* vol. 21, no. 5, pp. 528-534, 2015.

[74] Ultimaker, "What is g-code?," [Online]. Available: https://ultimaker.com/en/resources/39071-what-is-g-code. [Accessed 2018].

[75] Smooth-On Inc., "Silicone Rubber - Platinum Cure," [Online]. Available: https://www.smooth-on.com/category/platinum-silicone/. [Accessed 2018].

[76] Smooth-On Inc., "Durometer Shore Hardness Scale," [Online]. Available: https://www.smooth-on.com/page/durometer-shore-hardness-scale/. [Accessed 2018].

[77] FormX, "FFX LY-series," [Online]. Available: http://www.formx.es/hidden2/fuse-fx-series/ffx-ly-series/index.php. [Accessed 2018].

[78] HoloLens, "HoloLens Can Now Simulate Childbirth to Train Medical Students," [Online]. Available: https://hololens.reality.news/news/hololens-can-now-simulate-childbirth-train-medical-students-0182126/. [Accessed 2018].

[79] HoloLens, "HoloLens Assists in Live Surgery," [Online]. Available: https://hololens.reality.news/news/hololens-assists-live-surgery-0178887/. [Accessed 2018].

[80] D. I. Watson, P. J. Treacy and J. A. R. Williams, "Developing a training model for laparoscopic common bile duct surgery," *Surgical Endoscopy,* vol. 9, no. 10, pp. 1116-1118, 1995.